THE JOURNAL OF BIOLOGICAL CHEMISTRY VOL. 288, NO. 52, pp. 37241–37255, December 27, 2013
© 2013 by The American Society for Biochemistry and Molecular Biology, Inc. Published in the U.S.A.

The Prion Protein Modulates A-type K^+ Currents Mediated by Kv4.2 Complexes through Dipeptidyl Aminopeptidase-like Protein 6*

Received for publication, May 24, 2013, and in revised form, November 8, 2013 Published, JBC Papers in Press, November 13, 2013, DOI 10.1074/jbc.M113.488650

Robert C. C. Mercer[‡§1,2], Li Ma[§¶1], Joel C. Watts[‖], Robert Strome[‖], Serene Wohlgemuth[‡§], Jing Yang[‡], Neil R. Cashman[**], Michael B. Coulthart[‡‡], Gerold Schmitt-Ulms[‖], Jack H. Jhamandas[§¶3], and David Westaway[‡§¶§§4]

From the [‡]Centre for Prions and Protein Folding Diseases, the [§]Department of Medicine (Neurology), the [¶]Centre for Neuroscience, and the [§§]Department of Biochemistry, University of Alberta, Edmonton, Alberta T6G 2M8, Canada, the [‖]Tanz Centre for Research in Neurodegenerative Diseases, University of Toronto, Toronto, Ontario M5T2S8, Canada, the [**]Division of Neurology, University of British Columbia, Vancouver, British Columbia V6T2B5, Canada, and the [‡‡]Canadian Creutzfeldt-Jakob Disease Surveillance System, Public Health Agency of Canada, Ottawa, Ontario K1A0K9, Canada

Background: Prion protein (PrP) interacts with dipeptidyl aminopeptidase-like protein 6 (DPP6), but the functional significance was unknown.
Results: PrP formed complexes with and impacted the function of potassium channels containing DPP6 and Kv4.2.
Conclusion: PrP modulates voltage-dependent and kinetic properties of Kv4.2 channels.
Significance: This could explain a phenotype of PrP knock-out mice and the effects of amyloid β oligomers.

Widely expressed in the adult central nervous system, the cellular prion protein (PrP^C) is implicated in a variety of processes, including neuronal excitability. Dipeptidyl aminopeptidase-like protein 6 (DPP6) was first identified as a PrP^C interactor using *in vivo* formaldehyde cross-linking of wild type (WT) mouse brain. This finding was confirmed in three cell lines and, because DPP6 directs the functional assembly of K^+ channels, we assessed the impact of WT and mutant PrP^C upon Kv4.2-based cell surface macromolecular complexes. Whereas a Gerstmann-Sträussler-Scheinker disease version of PrP with eight extra octarepeats was a loss of function both for complex formation and for modulation of Kv4.2 channels, WT PrP^C, in a DPP6-dependent manner, modulated Kv4.2 channel properties, causing an increase in peak amplitude, a rightward shift of the voltage-dependent steady-state inactivation curve, a slower inactivation, and a faster recovery from steady-state inactivation. Thus, the net impact of wt PrP^C was one of enhancement, which plays a critical role in the down-regulation of neuronal membrane excitability and is associated with a decreased susceptibility to seizures. Insofar as previous work has established a requirement for WT PrP^C in the Aβ-dependent modulation of excitability in cholinergic basal forebrain neurons, our findings implicate PrP^C regulation of Kv4.2 channels as a mechanism contributing to the effects of oligomeric Aβ upon neuronal excitability and viability.

Prion diseases involve the structural conversion of the primarily α-helical, cellular prion protein (PrP^C)[5] to an infectious, β-sheet-enriched form, PrP^{Sc}. The high degree of primary to tertiary structural conservation of mammalian PrP^C (1, 2) leads to an expectation of an explicit phenotype in *Prnp*$^{0/0}$ mice, but, aside from a total resistance to prion disease, this is not the case (3, 4). That said, within the inventory of subtle or disputed phenotypic changes in these mice are reports of impairment in $GABA_A$ receptor-mediated inhibition and long term potentiation (5–8). The diversity of altered end point measures is, to a certain extent, paralleled in the large number of reported PrP^C-interacting proteins: the laminin receptor (9–11), the neural cell adhesion molecule (12, 13), stress-inducible protein-1 (14, 15), and NMDA receptors (16, 17) to name but a few (reviewed in Ref. 18).

In addition to previously described interacting proteins, dipeptidyl aminopeptidase-like protein 6 (DPP6; also known as DPPX) was identified using time-controlled transcardiac perfusion cross-linking while probing the PrP^C interactome (19). DPP6 is an auxiliary subunit of pore-forming Kv4.2 channels (20, 21) and, together with most K^+ channel-interacting protein (KChIP) isoforms (22), DPP6 increases Kv4.2 trafficking to the cell surface and is required for the reconstitution of the properties of the native channel complex in heterologous cells (23). A type II transmembrane protein, DPP6 has a number of splice variants differing in the length of the cytoplasmic, N-terminal portion (DPP6-S; short) (24). KChIPs are a family of

* This work was supported by grants from the PrioNet Network Centres of Excellence, Alberta Prion Research Institute Grant APRI 200600070, Alberta Innovates-Health Solutions Grant AHFMR 201000628, Canadian Institutes of Health Research Grants MOP36377 and 93601, and the Canadian Foundation for Innovation.
[1] Both authors contributed equally to this work.
[2] Recipient of Alberta Innovates-Health Solutions Scholarship AHFMR 201100104.
[3] To whom correspondence may be addressed: 530 Heritage Medical Research Centre, University of Alberta, Edmonton, Alberta T6G 2S2, Canada. Tel.: 780-407-7153; Fax: 780-407-3410; E-mail jack.jhamandas@ualberta.ca.
[4] To whom correspondence may be addressed: Centre for Prions and Protein Folding Diseases, 2-04 Brain and Aging Research Bldg., University of Alberta, Edmonton, Alberta T6G 2M8, Canada. Tel.: 780-492-9377; Fax: 780-492-9352; E-mail: david.westaway@ualberta.ca.

[5] The abbreviations used are: PrP^C, cellular prion protein; PrP, prion protein; DPP6, dipeptidyl aminopeptidase-like protein 6; KChIP, K^+ channel-interacting protein.

intracellular Ca^{2+}-binding proteins with four major isoforms (1–4) and at least 16 splice variants (25). Interactions between Kv4.2, KChIPs and DPP6 have been confirmed by proteomic analyses demonstrating the pull-down of KChIP1 to -3 in comparable ratios (26). Assembled Kv4 channel complexes mediate sub-threshold operation somatodendritic transient outward K^+ currents (A-type K^+ currents), which play important roles in the regulation of neuronal membrane excitability, somatodendritic signal integration, and long term potentiation (27, 28). Given the interplay between Kv4.2 channels and DPP6 in neuronal function (29) and the ability to cross-link DPP6 and PrP^C *in vivo* (19), we sought to delineate the nature and repercussions of a DPP6-PrP^C interaction. To this end, we investigated the impact of PrP^C upon the properties of A-type K^+ currents mediated by Kv4.2 channel complexes derived from co-expression of Kv4.2, KChIP2, and DPP6-S (30, 31).

EXPERIMENTAL PROCEDURES

Plasmid Construction—cDNAs encoding Kv4.2 (MMM1012-9498428 clone 30356567, pYX-Asc) and KChIP2 (MMM1013-7511937 clone 4503251, pCR4-TOPO) (Open Biosystems) were inserted behind the CMV and EF1α promoters, respectively, of pBud.CE4 with Quick Ligase (New England Biolabs) to create pBud.CE4.Kv4.2.KChip2. To construct pBud.DPP6-S.RFP (co-expression driven from the CMV and EF1α promoters, respectively), total RNA was isolated from half mouse brains using acid guanidinium thiocyanate/phenol/chloroform extraction (32) and mRNA-purified using the Oligotex mRNA minikit (Qiagen). cDNA synthesis was performed in the presence of SUPERase-In RNase inhibitor (Ambion) using 0.5 μg of mRNA, Omniscript reverse transcriptase (Qiagen), and an oligo(dT) primer. PCR amplification of DPP6-S and DPP6-E was conducted using *Pfu* Turbo DNA polymerase (Invitrogen) with a nested PCR strategy and inserted between the BamHI and XbaI sites of the pcDNA3 mammalian expression vector (Invitrogen). A PstI site was added to the pcDNA3.DPP6-S for insertion into pBud.empty.GFP with Quick Ligase (New England Biolabs) after gel purification (QIAquick gel extraction kit (Qiagen)). GFP was replaced with RFP by digestion of pBud.DPP6-S.GFP and pBud.empty.RFP with NdeI and NheI, isolation of the desired fragments, and ligation. HA-tagged DPP6-S, DPP6Δcyto, and DPP6 deletion mutants were generated by standard PCR-based techniques. The secreted DPP6 ectodomain construct was generated by fusing the DPP6 ectodomain to the PrP N-terminal signal sequence using an introduced BsrGI site. The Thy-1 plasmid (Thy-1.2 isoform) was generated by amplification of the Thy-1 open reading frame from the MGC:62652 cDNA clone by PCR and then insertion into pcDNA3. PrP A116V and M128V HD dup PrP were created using the QuikChange (Stratagene) site-directed mutagenesis procedure with *Pfu* Turbo DNA polymerase. Other PrP mutants and Doppel plasmids were generated as described previously (33). All plasmids used for transfection were enriched using the EndoFree Plasmid Maxi kit (Qiagen).

Transfections—HEK293T cells were maintained in DMEM with 10% FBS (Invitrogen). Transfections were performed with Lipofectamine 2000 (Invitrogen) according to the manufacturer's instructions. Cells used for electrophysiological recording were transfected with the following plasmids (fluorescent proteins co-expressed): pBud.DPP6-S.RFP, pBud.Kv4.2/KChIP2, pBud.wtPrP.GFP, pBud.octa13PrP.GFP, and pBud.empty.GFP. These transfection mixtures included (as noted) siRNA directed against the 3′-non-coding region of human *PRNP* mRNA (OriGene Trilencer-27 siRNA duplex; rGrGrCrUrUrArCrArArUrGrUrGrCrArCrUrGrArArUrCrGTT) or a scrambled control siRNA. 24 h after transfection, cells were trypsinized and plated on coverslips for electrophysiological recording the following day. Cells used for complex formation assays were transfected as above using constructs based on a pcDNA plasmid vector backbone (with identities indicated in the figure legends) except for Fig. 3*C*, which used a pBud vector.

Generation of DPP6 Antibodies—Peptides were synthesized (containing an N-terminal cysteine for KLH conjugation), conjugated to maleimide-activated KLH (Pierce), and then injected into New Zealand White rabbits. 03J2 was raised against residues 507–522 (DKRRMFDLEANEEVQK), and 03K1 was raised against residues 788–803 (QDKLPTATAKEEEEED). Polyclonal antibodies were precipitated from serum using ammonium sulfate and affinity-purified using the corresponding immunogenic DPP6 peptide conjugated to a SulfoLink column (Pierce).

Cell Surface Biotinylation Assay—The assay was performed according to the manufacturer's instructions (Pierce).

Formaldehyde Cross-linking of Intact Cells—24 h after transfection, cells (HEK293T, RK13, or N2a) were washed twice with PBS and incubated for 15 min at room temperature with 2 or 0.4% formaldehyde in PBS. The cross-linking reaction was quenched with 0.125 M glycine for 10 min. Lysis was performed with radioimmune precipitation assay buffer (50 mM Tris base, 150 mM NaCl, 0.1% SDS, 0.5% sodium deoxycholate, 1% Triton X-100) containing protease inhibitors (Roche Applied Science) at 4 °C.

Immunoprecipitations—120 μg of cell lysate was incubated overnight at 4 °C with 0.7 μg of α-HA antibody (Sigma) in a total volume of 50 μl. 100 μl of protein A/G-agarose beads were washed three times with radioimmune precipitation assay buffer containing protease inhibitor (Roche Applied Science) before adding the overnight incubation and were then incubated at room temperature for 2 h rotating end over end. After three washes with radioimmune precipitation assay buffer, the beads were washed a final time with water, and the complexes were eluted from the beads (and cross-links were reversed) by incubation in sample buffer at 95 °C for 30 min.

Animal Husbandry—All animal protocols were in accordance with the Canadian Council on Animal Care and were approved by the Institutional Animal Care and Use Committees at the University of Alberta and the University of Toronto.

Mouse Lines and Preparation of Mouse Brain Homogenates—*Prnp$^{0/0}$* mice (*ZrchI* strain) were maintained on a C57/B6 background. DPP6$^{df5J/Rw}$ mice were a generous gift from John Schimenti and were maintained on a C3H background. Mice were perfused with saline, and half-brains were extracted and then either homogenized directly in nine volumes of 0.32 M sucrose with protease inhibitors (Roche Applied Science) or snap-frozen and stored at −80 °C.

Time-controlled Transcardiac Perfusion Cross-linking—Mice (either C57/B6 or FVB strains) were subjected to time-controlled transcardiac perfusion cross-linking, as described previously (19). Brains were homogenized in 0.32 M sucrose containing protease inhibitor (Roche Applied Science).

Western Blotting—Cells were lysed with radioimmunoprecipitation assay lysis buffer. Brains were homogenized in 0.32 M sucrose. A BCA assay (Pierce) was performed to determine protein concentration. Samples were boiled in loading buffer (with the exception of samples to be used for Kv4.2 detection due to protein aggregation), and were electrophoresed with either Tris-glycine gels (8 or 12%) or 4–12% NuPAGE gradient gels (Invitrogen) and transferred to PVDF membranes (Millipore). Membranes were blocked with either 3% (Kv4.2) or 5% milk (all others except for SHA31 blots, which are not blocked) in TBS with 0.1% Tween (Fisher). Membranes were incubated overnight in the indicated primary antibody (DPP6 clones 03K1 and 03J2 (created in house), actin (Sigma), Kv4.2 clone K57/1 and KChIP2 clone K60/73 (NeuroMab), SHA31 (Spi-bio), 8B4 and 7A12 (generous gifts from Man-Sun Sy), HA (Sigma), and Thy-1 (graciously provided by Roger Morris)) and after washing were incubated in the appropriate HRP-conjugated secondary antibody for 2 h at room temperature (goat α-mouse or goat α-rabbit (Bio-Rad)), washed again, exposed to ECL (Pierce), and visualized with light-sensitive film (Fujifilm). Quantification was performed using ImageJ. The intensity of the ~191-kDa species detected by Western blotting was normalized to intensity of "monomeric input" PrP in the same gel lane and plotted using an arbitrary scale. p values were determined using Student's t test.

Immunocytochemistry—HEK293T cells were transfected with mouse PrP and HA-tagged DPP6-S (both on a pcDNA backbone) and an siRNA against endogenous human PrP. 24 h after transfection, cells were replated on glass coverslips and given 24 h to recover. After rinsing twice with PBS and fixation with 4% paraformaldehyde, cells were washed three times with PBS and incubated in Sha31 (1:5000) overnight at 4 °C with rocking. Following three PBS washes, cells were blocked with 2% goat serum (Invitrogen) and incubated with goat α-mouse Alexa Fluor 594 (1:300; Invitrogen) for 2 h at room temperature. After washing and permeabilization with 0.2% Triton X-100, cells were blocked and incubated overnight in 1:500 α-HA (Sigma) as above, washed three times, blocked, and incubated for 2 h with 1:300 goat α-mouse Alexa Fluor 488 (Invitrogen) at room temperature. Nuclei were stained with 1 μg/ml Hoechst and visualized using a Nikon Eclipse 90I motorized upright microscope (Nikon) and a CFI PL ×40/numerical aperture 0.75 lens (Nikon) using the following excitation/emission filter properties: 325–375/500–575 nm with a 495-nm long pass filter (blue channel), 440–510/475–575 nm with a 495-nm long pass filter (green channel), and 505–615/570–720 nm with a 595-nm long pass filter (red channel). Images were acquired with a Retiga 2000R monocooled camera, fast 1394, using NIS-Elements AR advanced research software at room temperature.

Recordings from HEK293T Cells—Whole-cell recordings were always applied to two groups of HEK293T cells on the same day to minimize variation resulting from cell manipulation prior to recordings. Fluorescence-positive individual HEK293T cells were visualized (by way of the GFP and RFP encoded in the bigenic plasmids) and selected for recording under an Axioscope 2 Fs microscope (Zeiss) at ×60 magnification. Oxygenated external solution was bath-perfused at a rate of 1.0 ml/min. The external solution contained 140 mM NaCl, 2.5 mM KCl, 1.2 mM $MgCl_2$, 1.5 mM $CaCl_2$, 10 mM HEPES, and 10 mM glucose, pH 7.4. Recording pipette solution was composed of 140 mM potassium methylsulfate, 5 mM $MgCl_2$, 10 mM HEPES, 2 mM Na_2ATP, 0.2 mM NaGTP, and 0.5 mM EGTA, pH 7.3. Borosilicate glass capillaries (thin wall with filament, 1.5 mm; World Precision Instruments) were pulled with a Narishige (PP-83) puller to yield recording pipettes with resistances of 2–4 megaohms. Series resistance of 4–7 megaohms in whole-cell configuration was compensated by 60%. Three different stimulation protocols in our experiments were employed to evoke Kv4.2-mediated A-type K^+ currents, which were used for building relationship of voltage-dependent activation (activation curve), steady-state inactivation (inactivation curve), and rate of recovery time from steady-state inactivation (curve of recovery time). A-type K^+ currents for making the activation curves were evoked for 300 ms, depolarizing membrane potential ranging from −60 to 50 mV following a conditioning pulse of −110 mV for 400 ms. The A-type K^+ currents used to build the inactivation curves were evoked during a fixed depolarizing potential of 30 mV following 400-ms conditioning pulses of various membrane potentials, ranging from −110 to −20 mV. A-type K^+ currents for plotting the curve of the recovery rate were elicited during a fixed 30-mV depolarizing membrane potential for 300 ms following a series of increasing time intervals of conditioning hyperpolarizing potential at −110 mV. All A-type currents presented were subject to subtraction of the outward currents (endogenous currents) evoked by a conditioning pulse of −20 mV from that evoked by any protocols mentioned above. The current signals were acquired at a bandwidth of 10 kHz using pClamp version 9.2 software and filtered with a 5-kHz low pass Bessel filter using an Axopatch 200B amplifier (Molecular Devices).

Data Analysis—Time to half-inactivation ($t_{1/2}$) is the time at which 50% of peak amplitude is inactivated at the indicated voltage. The activation curve was obtained by plotting normalized conductance of peak amplitude of A-type K^+ currents against its corresponding depolarizing membrane potential. The inactivation curve was built by plotting normalized peak amplitude of A-type currents against its corresponding conditioning membrane potential. The curve of recovery rate from steady-state inactivation was obtained by plotting the peak amplitude of A-type currents against its corresponding time intervals at a conditioning hyperpolarizing membrane potential of −110 mV. The time constant (t_{rec}) of recovery rate was measured by fitting the curve to a single exponential function. Average values were expressed as mean ± S.E., and statistical significance was evaluated by means of the two-tailed Student's unpaired t test. The significance level for the t tests was set at $p < 0.05$.

RESULTS

Determinants of Complex Formation between PrP^C and DPP6—To facilitate our analyses of DPP6 and DPP6-containing protein complexes, two polyclonal peptide antisera, 03K1 and 03J2,

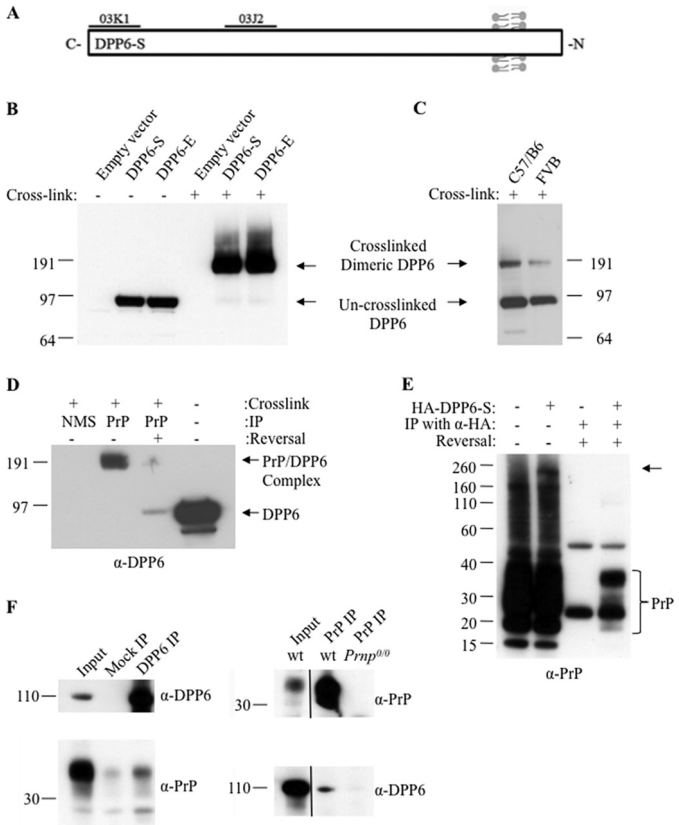

FIGURE 1. **DPP6 exists as a dimer and forms high M_r complexes with PrP^C.** *A*, schematic representation of DPP6-S with the approximate locations of antibody epitopes indicated. DPP6-S is a type II membrane protein and is presented in the form, HOOC-ectodomain, TM domain, cytoplasmic tail-NH_2, from *left* to *right*. *B*, transfected membrane-anchored DPP6 exists as a dimer in N2a cells. N2a cells were transfected with plasmids encoding the indicated proteins, cross-linked with 2% formaldehyde as indicated, lysed, and then analyzed by Western blotting with 03J2. Cross-linked dimeric DPP6 is the main species observed. *C*, DPP6 exists as a dimer in WT mouse brains. Brains from mice of the indicated strain were cross-linked *in vivo* using the time-controlled transcardiac perfusion crosslinking procedure and analyzed by Western blotting 03J2. A signal at ~191 kDa is apparent, indicative of dimeric DPP6. *D*, immunoprecipitation (*IP*) of DPP6 by 7A12 (α-PrP). N2a cells were transfected with DPP6-S, cross-linked with 2% formaldehyde, and lysed, and then immunoprecipitations were performed with either normal mouse serum (*NMS*) or 7A12. Following pull-down, a band reactive to DPP6 antibodies was observed, indicative of complex formation between PrP^C and DPP6-S. After cross-link reversal, a signal was obtained compatible with full-length glycosylated DPP6 monomers. *E*, immunoprecipitation of PrP^C by α-HA. N2a cells were co-transfected with HA-tagged DPP6-S and PrP^C. Following cross-linking with 2% formaldehyde, high M_r complexes are observed (*arrowhead*). PrP^C·DPP6 complexes were isolated by immunoprecipitation using α-HA, and then cross-links were reversed. *F*, reciprocal co-immunoprecipitation of DPP6 and PrP^C from non-cross-linked mouse brain. Detergent-extracted wild-type mouse brain homogenates were subjected to immunoprecipitation with either 03K1 (*left panels*) or 8B4 (*right panels*).

were raised in rabbits (Fig. 1*A*). Western blot analysis of brain homogenate from WT and DPP6-deficient mice (DPP6$^{df5J/Rw}$) (34) assessed specificity (not shown), revealing immunoreactive species of ~110 kDa in accord with glycosylation of full-length DPP6 (~91 kDa) (35). Immunohistochemistry demonstrated the widespread expression of DPP6 in the mouse brain (not shown), confirming previous reports (36). The crystal structure of recombinant DPP6 is dimeric (35), and protein species with an electrophoretic mobility consistent with dimers were observed in transfected cells and mouse brain homogenate after cross-linking and analysis by Western blot (Fig. 1, *B* and *C*). When N2a cells expressing endogenous PrP^C were transfected with plasmids encoding DPP6 (DPP6-S and DPP6-E) (23), cross-linked, and immunoprecipitated with 7A12 (α-PrP) and membranes were probed with 03K1, a novel species was observed with a mobility of ~190 kDa (Fig. 1*D*). These data indicate that PrP^C is located in membrane subdomains that harbor dimeric DPP6 or that PrP and DPP6 exist in direct physical contact in a protein complex with a stoichiometry that totals to an M_r of ~190,000. Reversal of cross-links yielded a species that co-migrated with full-length glycosylated DPP6-S. In a reciprocal analysis, following cross-linking, cells expressing HA-tagged DPP6-S yielded high M_r species and, after reversal, a signal compatible with glycosylated PrP^C (Fig. 1*E*). Co-immunoprecipitation was also achieved in WT mouse brain without cross-linking using either 8B4 (α-PrP) or 03K1 for pull-down (Fig. 1*F*).

Subsequently, mutant alleles were used to map regions within PrP^C and DPP6 required for association (Figs. 2*A*, 3*A*, and 4*A*). Deleting the intracellular, N-terminal portion of DPP6 ("DPP6Δcyto") had no effect upon complex formation with PrP^C (Fig. 2, *A*, *B*, and *E*). "secDPP6," where DPP6 residues 56–803 are prefaced by the PrP N-terminal signal peptide, causing secretion from the cell, was not associated with complex formation with PrP^C (Fig. 2, *A*, *C*, *E*, and *F*). Because this secDPP6 allele was readily detected in the culture medium, this implies a requirement for membrane association for complex formation rather than presence in the extracellular milieu. Also, anchoring to the membrane by a glycosylphosphatidylinositol moiety was not sufficient for complex formation because the assay failed to detect DPP6·Thy-1 complexes (37) (Fig. 2*D*).

To delineate the role of the DPP6 ectodomain (35) in complex formation with PrP^C, we used a series of DPP6 deletions with an N-terminal HA tag (Fig. 3*A*). Control experiments confirmed that these DPP6 constructs were expressed at the cell surface (Fig. 3*B*), and following cross-linking and immunoprecipitation with an α-HA antibody, cross-links were reversed before blot analysis. PrP^C was recovered in conjunction with all DPP6 deletion mutants tested (Fig. 3*C*), leading to the inference that DPP6 residues 56–80 contribute to complex formation. This was investigated further by performing the cross-linking assay with an internally deleted form of DPP6 Δ56–81 (this deletion covers the same interval but extends one residue further to isoleucine 81 to maintain the length of the hydrophobic TM region). For DPP6 Δ56–81, the ability to form complexes was lower than for WT DPP6 (Fig. 3*D*), underscoring a role for the juxtamembrane region.

With regard to PrP, N-terminal deletions Δ23–88 and Δ32–121, which encompass most or all of the octarepeats, had subtle effects on complex formation (Fig. 4, *A*, *B*, and *E*). The contribution of an interval that encompasses the first β-strand of the PrP structure (38, 39) to complex formation with DPP6 is illustrated by the performance of the Δ32–134 PrP allele (Fig. 4, *A* and *B*). We also created PrP alleles with more C-terminal deletion intervals; aside from theoretical caveats (see "Discussion"), these were also limited by lower expression levels than WT PrP and were not examined further. A survey of PrP alleles from genetic prion diseases defined a striking result associated with

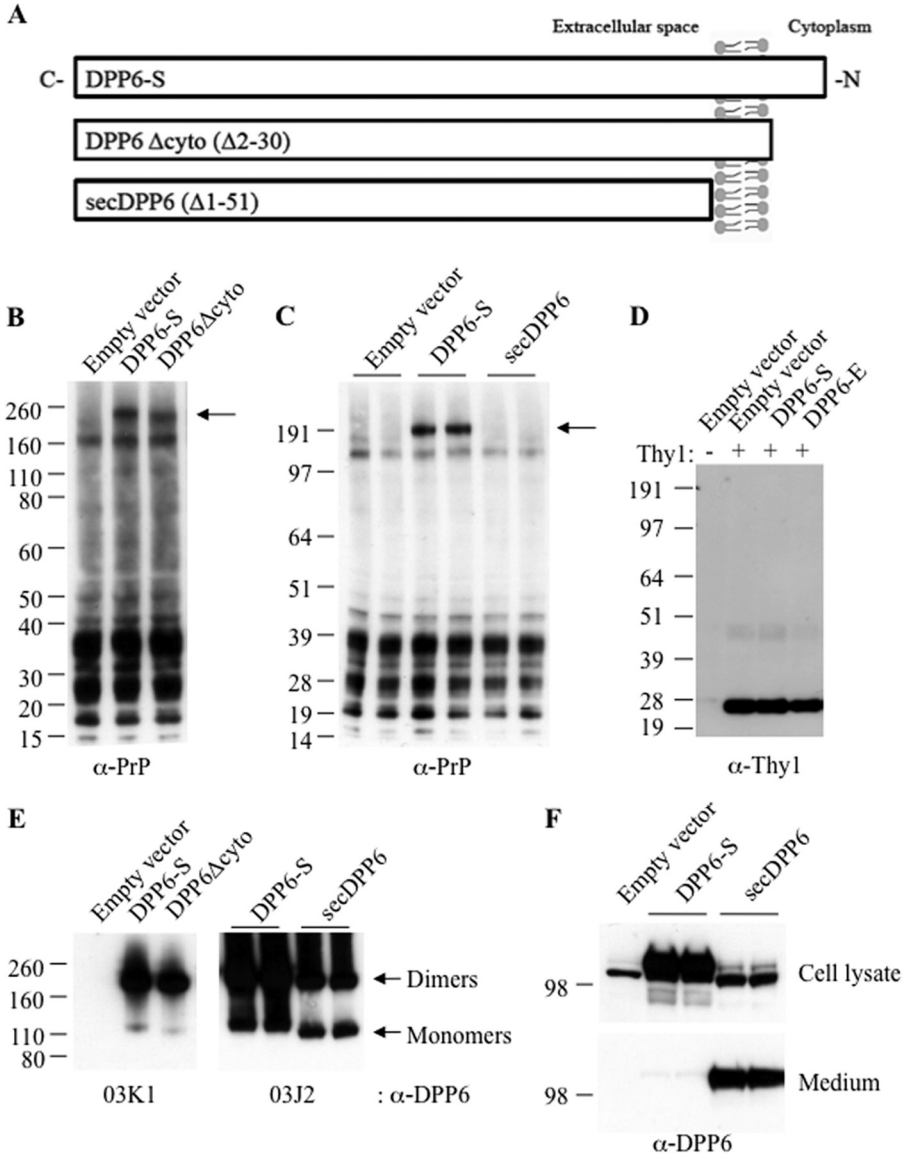

FIGURE 2. **Membrane anchorage of DPP6 is required for complex formation with PrP^C.** *A*, schematic representation of DPP6 mutants. DPPXΔcyto lacks all but three residues of the cytoplasmic domain, whereas secDPPX directs the secretion of the DPP6 ectodomain into the lumen/extracellular space. *B–F*, N2a cells were transfected with the indicated plasmids, cross-linked with 2% formaldehyde, and lysed, and complexes (*arrows*) were analyzed by Western blotting. *B* and *C*, the cytoplasmic domain of DPP6 is not required for complex formation with PrP^C, whereas the secreted DPP6 ectodomain fails to form a complex with PrP^C. *D*, no high *M*, complexes are observed between Thy-1 and DPP6. *E*, both DPP6Δcyto and secDPP6 are capable of forming dimers. *F*, minimal amounts of wild-type DPP6-S are present in the conditioned medium, whereas large amounts of secDPP6 are found in this fraction. Accordingly, a smaller proportion of secDPP6 is found in the cell lysate.

the octarepeat region (33, 41) but not with mutations C-terminal to this position (42–44). octa13 PrP, an expansion of the octarepeats to a total of 13, was less efficient than WT PrP at complex formation with DPP6 (Fig. 4, *A*, *C*, and *D*). Densitometry revealed that octa13 PrP formed ~191-kDa complexes at a level of 23.3 ± 16.4% that of WT PrP (100 ± 12.4%; $n = 3$, $p < 0.002$). As a preface to the functional studies described below, this result was confirmed in cross-linking studies of HEK293T cells (Fig. 4*D*). Furthermore, we confirmed that full-length HA-tagged DPP6-S and PrP^C co-localize at the cell surface of the HEK293T cells used for electrophysiology (Fig. 4*F*). Last, interactions between PrP^C and DPP6 were found to take place in *cis* in a cell biological sense, as demonstrated by the lack of complex formation when cells expressing PrP^C or DPP6 are co-cultured before cross-linking and lysis (Fig. 4*G*). Interestingly, Doppel, with a three-dimensional fold similar to that of the PrP^C C terminus (40), can also form complexes with DPP6 isoforms (Fig. 5).

PrP^C Modulates A-type K$^+$ Currents Mediated by Kv4.2 Channel Complexes—Following co-expression of the components of the Kv4.2 channel complex (Kv4.2, KChIP2, and DPP6-S; Fig. 6*A*), whole-cell recordings were performed on transiently transfected HEK293T cells. Two series of A-type K$^+$ currents mediated by the Kv4.2 channel complex were investigated in the presence and absence of exogenous PrP^C (the isolate of HEK293T cells used here expressed endogenous human PrP^C; Figs. 6*A*, 8*A*, 9*A*, and 10*A*). As seen in Fig. 6*B*, an A-type outward K$^+$ current was generated in response to depolarizing

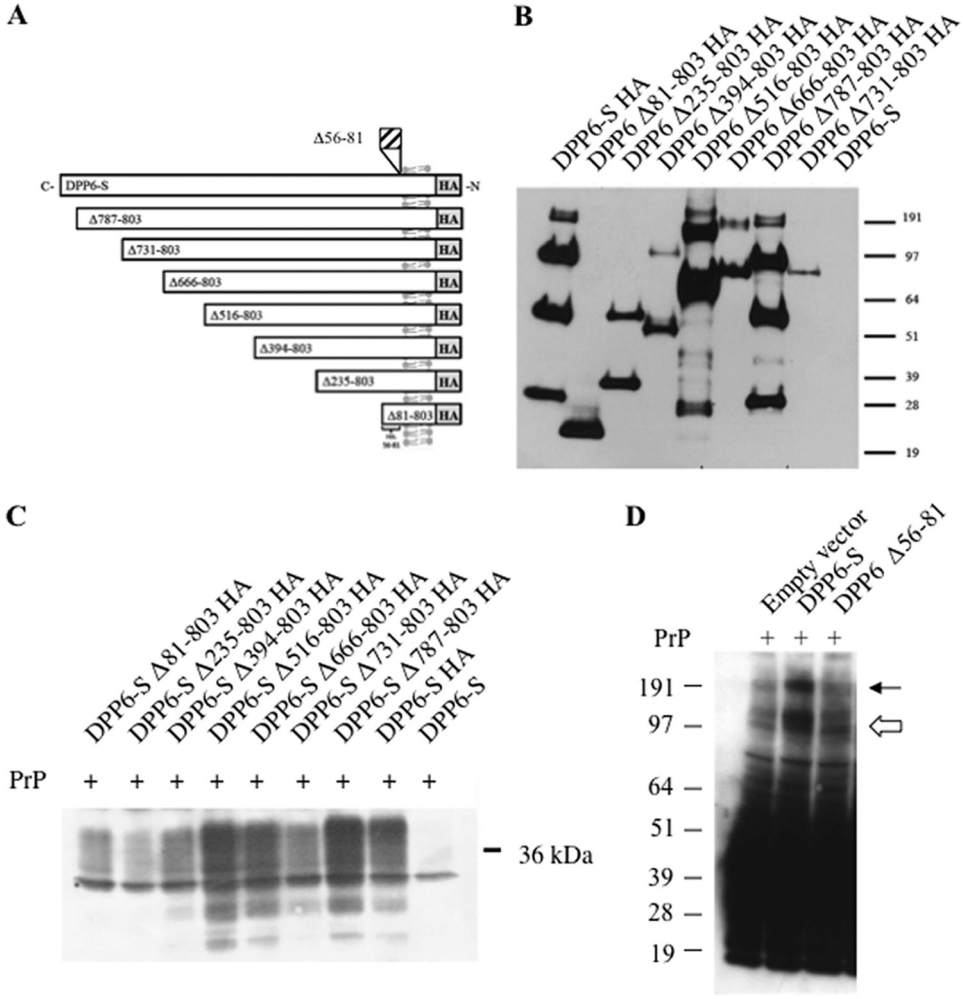

FIGURE 3. **DPP6-S determinants of complex formation with PrP^C.** *A*, schematic of sequential C-terminal DPP6-S deletion intervals. The internal deletion interval Δ56–81 inserted into WT DPP6-S is also shown (*cross-hatching*). *HA*, hemagglutinin epitope tag. *B*, DPP6 truncations are expressed on the cell surface. Transfected cells were treated with a commercial cell surface biotinylation kit, and avidin-captured proteins were run on a 4–12% NuPAGE gel. Western blots were performed with an α-HA antibody. Lower M_r bands are inferred to represent fragments that retain the HA tag but not the C-terminal epitopes that were used for polyclonal antibody generation. *C*, HA tag immunopurification assay to assess co-precipitation of PrP^C. *D*, Western blot demonstrating a lack of complex formation between DPP6 Δ56–81 and PrP^C. RK13 cells were transfected with PrP and the indicated form of DPP6, cross-linked with 0.4% formaldehyde, lysed, and analyzed using Sha31 (α-PrP). *Black arrow*, ~191-kDa complex; *open arrow*, ~100-kDa complex.

potentials. Following a rapid rise to peak amplitude, the current rapidly decayed despite a continued depolarizing step command. In the presence of exogenous PrP^C, the peak amplitude of the A-type K$^+$ currents at 20 mV was larger (14.5 ± 0.9 nA; average ± S.E., $n = 17$) than that mediated by the Kv4.2 channel complex in its absence (10.2 ± 1.0 nA; $n = 21$, $p < 0.05$) (Fig. 6*C*). The curve of voltage-dependent activation of A-type K$^+$ currents mediated by Kv4.2 channel complexes in the presence (*triangles*) and absence (*squares*) of exogenous PrP^C was created by plotting averaged normalized conductance (G/G_{max}) against corresponding depolarizing potential (Fig. 6*D*). There was no significant difference in the voltage-dependent activation between the two groups.

To establish voltage-dependent steady-state inactivation, A-type K$^+$ currents were evoked by another voltage stimulus protocol (see "Experimental Procedures"). To highlight differences, we have shown two traces of A-type K$^+$ currents mediated by the Kv4.2 channel complex alone (*left*) and with exogenous PrP^C (*right*) at conditioning potentials of −110 and −60 mV, respectively (Fig. 6*E*). The ratio of normalized peak amplitudes of the currents evoked at conditioning potentials of −60 and −110 mV was 0.29 in the absence of PrP^C *versus* 0.56 in its presence. The plot for voltage-dependent steady-state inactivation was obtained by plotting corresponding average normalized currents (I/I_{max}) against conditioning potential in the presence (*triangles*) and absence of exogenous PrP^C (*squares*) (Fig. 6*F*). Significant differences between these two groups were noted at conditioning potentials of −50, −60, and −70 mV ($n = 10$, $p < 0.05$).

To measure decay of A-type K$^+$ current from peak amplitude to base line, we used the time at which 50% of peak amplitude was inactivated at a given depolarizing potential (half-inactivation time) to quantitatively describe the time course for inactivation (20). Two representative traces of A-type K$^+$ currents evoked by a depolarizing potential of 50 mV in Fig. 6*B* are shown with an expanded time scale and correspond to the Kv4.2 channel complex with or without exogenous PrP^C (Fig. 7*A*). The half-inactivation time was increased from 17.6 to 31.2

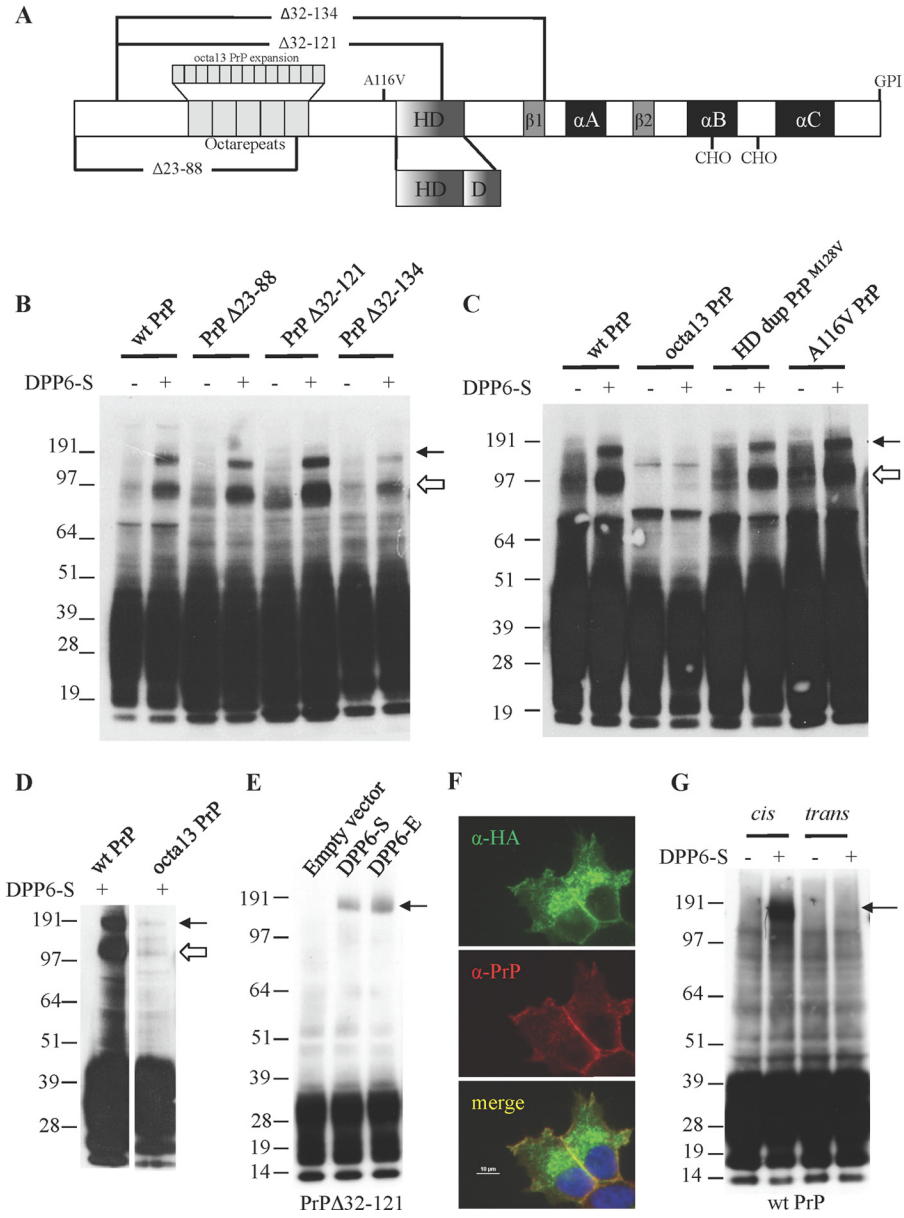

FIGURE 4. **PrP^C determinants of complex formation with DPP6-S.** *A*, schematic representation of PrP indicating deletion intervals, point mutations, the octa13 expansion, and a partial duplication of the hydrophobic domain found in a Canadian GSS patient (*HD Dup PrP*). *B* and *C*, Western blots demonstrating complex formation between DPP6 and allelic forms of PrP^C. RK13 cells were transfected with the indicated PrP forms and DPP6-S, cross-linked with 0.4% formaldehyde, lysed, and analyzed using Sha31 (α-PrP). *Black arrow*, ~191-kDa complex; *open arrow*, ~100-kDa complex. The intensity of the ~191 kDa band is expressed as a percentage, relative to WT PrP (value ± S.D.). *B*, WT PrP, 100 ± 28.0%; PrP Δ23–88, 70.3 ± 24.2% ($n = 3$, $p > 0.1$); PrP Δ32–121, 102.6 ± 18.4% ($n = 3$, $p > 0.4$); PrP Δ32–134, 43.4 ± 31.1% ($n = 3$, $p < 0.05$). *C*, WT PrP, 100 ± 12.4%; octa13 PrP, 23.3 ± 16.4% ($n = 3$, $p < 0.002$); M128V HD dup PrP, 85.0 ± 15.3% ($n = 3$, $p > 0.1$); PrP A116V, 94.4 ± 13.4% ($n = 3$, $p > 0.3$). *D*, HEK 293 T cells were co-transfected with DPP6-S and the indicated PrP plasmids and cross-linked with 0.4% formaldehyde. Intensity of the ~191 kDa band is expressed in arbitrary units: WT PrP, 100 ± 8.3%; octa13 PrP, 6.7 ± 3.7%. *E*, HEK293T cells were co-transfected with PrP Δ32–121 and the indicated DPP6 plasmids and cross-linked with 2% formaldehyde; PrP Δ32–121 was capable of forming complexes with both DPP6 isoforms. *F*, co-localization of PrP^C and HA-DPP6 in HEK293T cells as assessed by immunofluorescent labeling with Sha31 (α-*PrP*) and α-HA. *Scale bar*, 10 μm. *G*, PrP^C·DPP6 complexes result from interactions occurring within the same cell. HEK293T cells were either co-transfected with PrP^C and DPP6-S (in *cis* with respect to cellular disposition) or singly transfected with either PrP^C or DPP6-S (in *trans* with respect to cellular disposition). 24 h post-transfection, cells were trypsinized and replated either alone (*cis*) or with PrP^C and DPP6-S singly transfected cells mixed together (*trans*). After an additional 24-h incubation (at which time the cells were confluent), cells were cross-linked with 2% formaldehyde, and lysates were analyzed by blotting. PrP^C·DPP6 complexes (*arrow*) are only formed when PrP^C and DPP6 are present in the same cell (*i.e.* co-transfected).

ms by the presence of exogenous PrP^C. On average, the half-inactivation time of A-type K$^+$ currents mediated by Kv4.2 channel complexes in the presence of exogenous PrP^C ($n = 8$) was significantly longer than that mediated by the Kv4.2 channel complex alone ($n = 10$) at all but two depolarizing potentials (Fig. 7*B*; $p < 0.05$).

We noted above (Fig. 6*F*) for HEK293T cells expressing Kv4.2 complexes that when the conditioning potential applied is more positive than −40 mV, it is not possible to evoke an A-type K$^+$ current by stepping to a depolarizing potential of 30 mV. This status can be referred to as complete voltage-dependent steady-state inactivation of Kv4.2 channels and can be

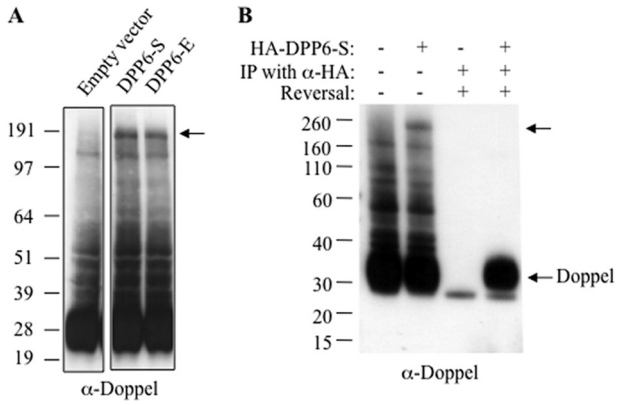

FIGURE 5. **The prion protein family member Doppel can also form complexes with DPP6.** *A*, N2a cells were co-transfected with Doppel and the indicated plasmids and cross-linked with formaldehyde. *B*, analysis of Doppel in high M_r complexes with DPP6. N2a cells were co-transfected with DPP6-S-HA and Doppel. Following cross-linking, high M_r complexes are observed (*arrow*). Complexes were isolated by immunoprecipitation (*IP*) using α-HA, and then cross-links were reversed (by boiling).

removed by first stepping to a conditioning hyperpolarizing potential (*e.g.* −110 mV) for a short duration. Consequently, to measure how fast A-type currents can recover from complete voltage-dependent steady-state inactivation, we recorded A-type K^+ currents evoked by a different stimulus protocol (Fig. 7*C*). Representative traces of the resulting A-type K^+ currents are shown for the presence and absence of exogenous PrP^C (Fig. 7*C*) with conditioning potentials of −110 mV for 5 and 170 ms, respectively. The ratios of the amplitudes of the currents measured with a pulse duration of 5-ms *versus* 170 ms at conditioning potentials of −110 mV were 0.24 (without) and 0.58 (with exogenous PrP^C). The average recovery rate from steady-state inactivation was obtained by plotting the time of conditioning hyperpolarizing potential at −110 mV against corresponding normalized currents (I/I_{max}) (Fig. 7*D*). The recovery rate was significantly faster in the presence of exogenous PrP^C ($n = 8$) than in its absence ($n = 10$) at the first two time intervals of 5 and 25 ms ($p < 0.05$). In both groups, recovery from steady state was virtually complete after 100 ms following a conditioning hyperpolarizing potential of −110 mV.

PrP^C Complex Formation with DPP6-S Is Required for Modulation of Kv4.2 Channel Properties—To ascertain whether or not the effects of PrP^C in this system are mediated through DPP6-S, we characterized the modulatory properties of PrP^C upon Kv4.2-mediated A-type K^+ currents in the absence of co-expressed DPP6-S (Fig. 8*A*). These A-type K^+ currents showed smaller peak amplitudes, a right shift of the activation curve, a right shift of the steady-state inactivation curve, a longer half-inactivation time, and a slower recovery rate from steady-state inactivation. These changes in the properties of A-type K^+ currents without DPP6-S are consistent with the previous findings observed by another group (24). However, exogenous PrP^C did not have a significant effect upon any A-type K^+ current properties in the absence of DPP6-S (Fig. 8, *B–F*).

Next, we studied the impact of co-expression of octa13 PrP (Fig. 4*A*) with Kv4.2 complexes that include DPP6-S. Although the stimulus protocols for these studies remained the same as in previous recordings (with the exception of those used to investigate recovery rate from steady-state inactivation; Fig. 7, *C* and *D*), we adjusted two aspects of the experimental design. First, the time interval for conditioning hyperpolarizing potential was reduced from the previous 20 ms to 5 ms to acquire more data points. Second, we used siRNA against human PrP mRNA to reduce the levels of endogenous PrP^C (Fig. 9*A*); by this means, we reduced cross-talk from WT PrP^C that could complicate the interpretation of data associated with transgene-encoded PrP. In this experimental context, WT PrP^C was found to modulate the Kv4.2 channel complex in the same manner as our previous data (Fig. 9, *B–F*). However, the properties of A-type K^+ currents in the presence of octa13 PrP showed no significant difference from those mediated by the Kv4.2 channel complex alone (Fig. 9, *B–F*, and Table 1). These data indicate that octa13 PrP is a loss of function with regard to modulation of Kv4.2, a finding that parallels its >75% loss in efficiency at forming cross-linked complexes with DPP6-S (Fig. 4, *C* and *D*).

In a final set of analyses, we further investigated the inference that residues 56–80 of DPP6 are required for complex formation with PrP^C. A-type K^+ currents mediated by the Kv4.2 complex composed of Kv4.2, KChIP2, and DPP6 Δ56–81 showed smaller peak amplitudes, a right shift of the activation curve, a right shift of the steady-state inactivation curve, a longer half-inactivation time, and a slower recovery rate from steady-state inactivation (Fig. 10). These changes in the properties of A-type K^+ currents are similar to those observed in the absence of DPP6-S (Fig. 8), indicating that DPP6 Δ56–81 is not fully functional. However, exogenous PrP^C did not modulate the properties of these A-type K^+ currents, further supporting the idea that this juxtamembrane region of DPP6 is required for complex formation with PrP^C (Figs. 3 and 10).

DISCUSSION

PrP^C and Ion Channels—PrP^C is highly expressed in the central nervous system (45–47), and consequently, its role in regulating neuronal excitability is of great interest. Prior studies have centered upon perturbations in electrophysiological recordings made from brain slices of *Prnp$^{0/0}$* mice (5–8, 16, 17, 48–51). Here we have investigated the influence of PrP^C upon Kv4.2 channel complexes by their reconstitution in HEK293T cells to study the currents produced by these complexes in isolation. These cells have been reported to have small endogenous delayed rectifier K^+ currents (52). We found identical currents in our HEK 293T cell isolate (generally smaller than 200 pA) but did not detect A-type K^+ currents, as previously reported by another group (53). Therefore, the A-type K^+ currents produced here (and measuring in the nanoampere range) by reconstitution of the Kv4.2 channel complex are not contaminated by the presence of endogenous currents. More recently, expression of PrP Δ105–125 in transfected cells has been reported to induce spontaneous non-selective, cation-permeable ion currents (54, 55). In this instance, because of the striking nature of the effect observed in HEK293T cells, we undertook parallel studies with the same allele inserted in our expression vectors, but none displayed a spontaneous ionic current ($n = 10$). To observe the currents, the cells were held at either −80 or +80 mV for several min. Under these conditions,

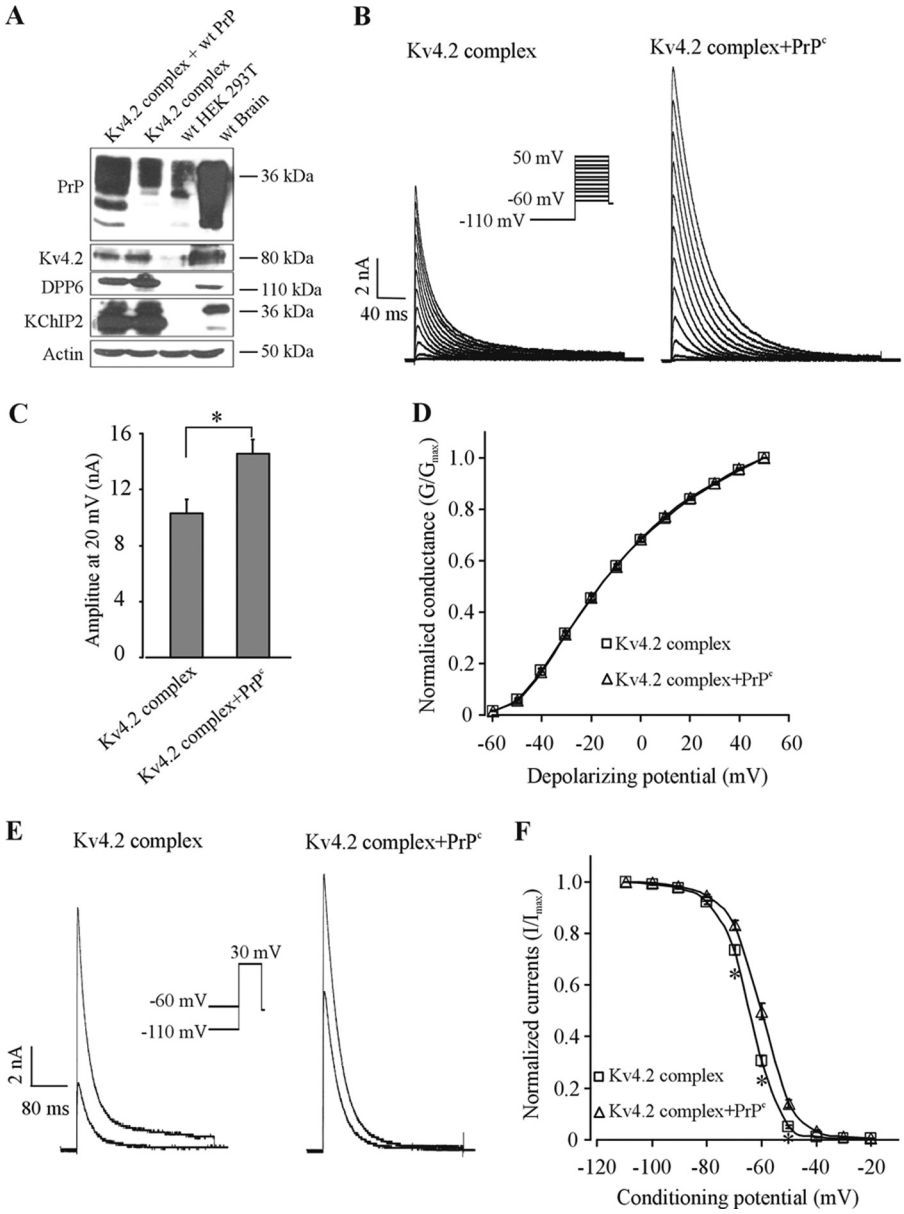

FIGURE 6. **PrP^C modulates the voltage-dependent properties of Kv4.2-mediated A-type currents in HEK293T cells.** *A*, Western blots demonstrating the presence or absence of the channel components. *B*, a series of A-type K^+ currents evoked by a stimulation protocol (*inset*) in cells transfected with the Kv4.2 channel complex with (*right*) and without exogenous PrP^C (*left*). *C*, average peak amplitude of A-type K^+ currents recorded at depolarizing potential of 20 mV with ($n = 21$) and without exogenous PrP^C ($n = 17$). *D*, average voltage-dependent activation of A-type K^+ currents with (*triangles*; $n = 8$) and without (*squares*; $n = 10$) exogenous PrP^C. *E*, sample traces of A-type K^+ currents evoked by a stimulation protocol (*inset*) with (*right*) and without exogenous PrP^C (*left*). *F*, the curves of averaged voltage-dependent steady-state inactivation of A-type currents with (*triangles*; $n = 10$) and without (*squares*; $n = 10$) exogenous PrP^C. *, significant difference at a given depolarizing or conditioning potential between the two groups ($p < 0.05$). *Error bars*, S.E.

it would be unlikely to miss any spontaneous current activity (54, 55). These experiments were performed both at 23 and 34 °C and with pipette solutions containing either 0.5 mM EGTA or 10 mM EGTA (54, 55). Although these data (not shown) did not support the concept of a solitary action of PrP for this particular allele under our designated experimental conditions, WT PrP^C impacted the performance of co-expressed DPP6·Kv4.2 complexes, as elaborated below.

In prior analyses, PrP^C has been implicated in the modulation of a variety of ion channels, including $GABA_A$ receptor/channels (5, 6, 8), calcium-dependent K^+ channels, and NMDA receptors/channels (16, 17, 48, 56, 57); stress-inducible protein-1-dependent intracellular Ca^{2+} fluxes mediated by the α7 nicotinic acetylcholine receptor (14, 15, 58); and an AMPA-dependent Zn^{2+} reuptake phenomenon (59). Remarkably, these studies convey a diversity of mechanisms whereby PrP^C modulates ion channels and neuronal excitability. For instance, enhanced and drastically prolonged NMDA-evoked currents in PrP^C knock-out mouse neurons were the result of a functional up-regulation of NMDA receptors containing NR2D subunits (16). On the other hand, impaired and depressed Ca^{2+}-dependent after-hyperpolarization potential in PrP^C knock-out mouse neurons arises from an increased intracellular Ca^{2+} buffering capability (48, 57). In this case, the free Ca^{2+} through influx of activated voltage-gated Ca^{2+} channels is decreased and in turn depresses the after-hyperpolarization potential.

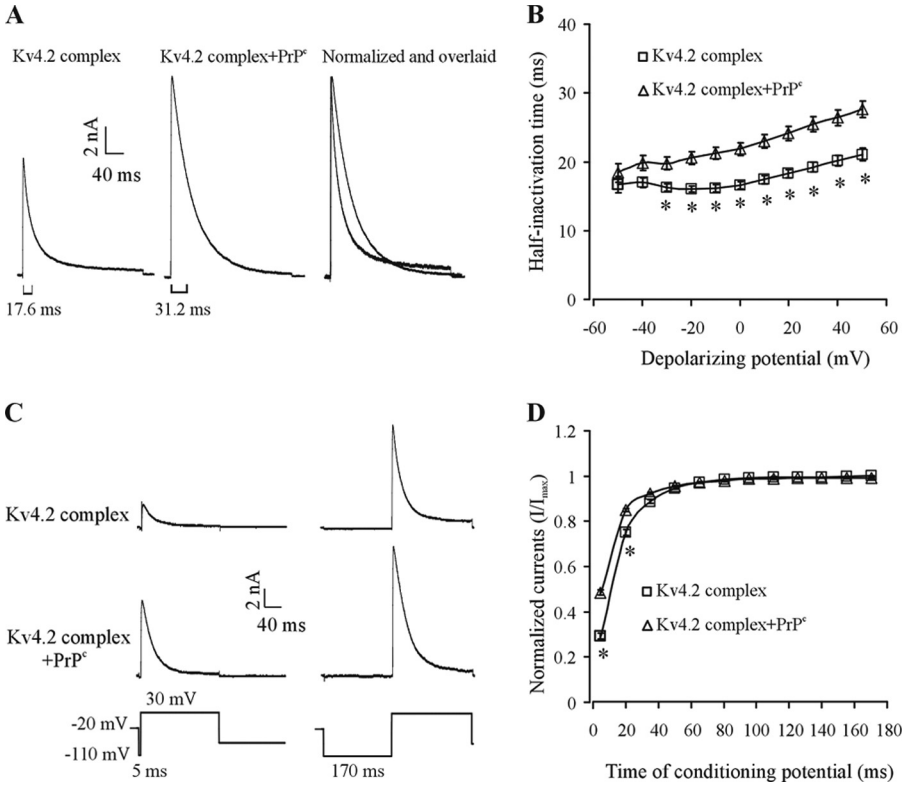

FIGURE 7. **PrP^C modulates time-dependent properties of Kv4.2-mediated A-type K$^+$ currents in HEK293T cells.** *A*, replotted traces of A-type K$^+$ currents obtained from Fig. 6*B* evoked by a depolarizing potential of 50 mV in cells without exogenous PrP^C (*left*), with exogenous PrP^C (*middle*), and normalized and overlaid (*right*). Note that the time to half-inactivation is increased in the presence of PrP^C. *B*, average half-inactivation time of A-type K$^+$ currents recorded at different depolarizing potentials with (*triangles*; $n = 8$) and without (*squares*; $n = 10$) exogenous PrP^C. *C*, traces of A-type K$^+$ currents evoked by a stimulus protocol (*bottom*), consisting of conditioning hyperpolarizing potential of −110 mV for 5 and 170 ms, respectively, with (*middle*) and without (*top*) exogenous PrP^C. Note that the normalized amplitude of the current recorded with a 5-ms conditioning hyperpolarizing potential to that with 170 ms is smaller in the absence of exogenous PrP^C. *D*, average curves of recovery rate from steady-state inactivation were created by plotting normalized peak currents (I/I_{max}) against the corresponding time interval of conditioning hyperpolarizing potential in the presence (*triangles*; $n = 8$) and absence (*squares*; $n = 10$) of exogenous PrP^C. *, significant difference at a given depolarizing potential or time interval of conditioning hyperbolizing potential in the two groups ($p < 0.05$). *Error bars*, S.E.

Here, the modulation of Kv4.2 properties by PrP^C requires interaction with DPP6-S and indicates that yet another, presently unknown, mechanism is employed. One possibility is increased trafficking of DPP6-S in the presence of PrP^C. A larger current amplitude and a faster recovery time from steady-state inactivation can be attributed to an increase of DPP6-S at the cell surface (20). However, the modulation of the voltage dependence of inactivation and half-inactivation time by PrP^C in this study counters the effect of DPP6-S. This suggests that the modulation of these channels by PrP^C occurs, at least partially, in a manner distinct from trafficking. Before addressing the puzzle presented by the pleiotropic actions of PrP^C, we will first consider molecular and mechanistic aspects of the PrP^C/A-type current paradigm.

PrP^C and the Kv4.2 Channel Complex—In genetic mapping of determinants necessary for PrP^C-DPP6 interactions (Figs. 1–5), WT N-terminal sequences up to residue 121, which are considered natively unstructured in the unmetallated form of PrP (39, 60), were not required. Deletions that begin to encroach on the C-terminal globular domain diminished the interaction (Fig. 4*B*). Although there are certain caveats concerning expression levels, chaperone interactions, and global folding that apply to the use of C-terminal deletions (61, 62), as yet we have been unable to find a crucial, common segment of PrP that is required for complex formation. We infer that a natively structured PrP^C globular domain (rather than a linear "epitope") is essential for complex formation. This is supported by the finding that Doppel also forms high molecular weight complexes with DPP6 (Fig. 5). For DPP6-S, the intracellular portion had no effect on complex formation with PrP^C, but there was a requirement for anchoring to the cell membrane (Fig. 2). With progressive ectodomain deletions, we determined that residues 1–81 retained the ability to immunoprecipitate PrP^C following cross-linking (Fig. 3, *A*–*C*). Because the 55 N-terminal residues of DPP6-S are found either on the cytoplasmic side of or spanning the membrane (and thus inaccessible to PrP^C), these data lead to an inference that the DPP6-S juxtamembrane region (residues 56–80) either complexes directly with the globular domain of PrP or is retained in PrP-enriched membrane domains by the action of an intermediary protein. This inference was bolstered by analyses of cells expressing an internal deletion (residues 56–81) incorporated into full-length DPP6-S (Fig. 3, *A* and *D*). These findings have a potential parallel in analyses and complement data indicating that the extracellular portion of DPP6 is not necessary for modulation of Kv4.2 channel properties (63).

Membrane Protein Assemblies and Pleiotropic Actions of PrP^C—To explain the curiously diverse actions of PrP^C in different experimental paradigms, Linden *et al.* (64) hypothesized its action as a dynamic scaffold at the cell surface, one that not

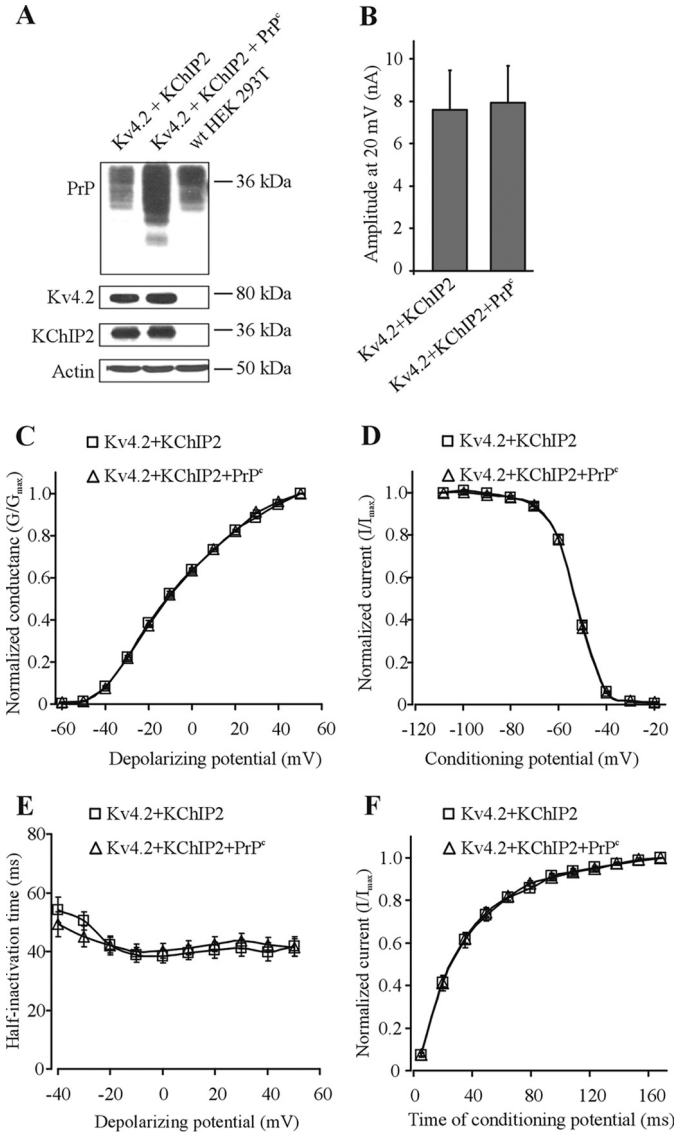

FIGURE 8. **Modulation of Kv4.2-mediated A-type K$^+$ a current by PrP^C is dependent upon the presence of DPP6-S.** *A*, Western blots demonstrating the presence or absence of channel components. *B*, average peak amplitude of A-type K$^+$ currents mediated by Kv4.2 + KChIP2 and by Kv4.2 + KChIP2 + exogenous PrP^C. *C*, average curves of voltage-dependent activation of A-type currents. *D*, averaged curves of voltage-dependent steady-state inactivation time of A-type currents. *E*, averaged half-inactivation times of A-type currents. *F*, averaged curves of recovery rate from steady-state inactivation of A-type currents. For *B–F*, data are from Kv4.2 + KChIP2-transfected cells (*squares*; $n = 8$) *versus* cells expressing Kv4.2 + KChIP2 + exogenous PrP^C (*triangles*; $n = 9$). *Error bars*, S.E.

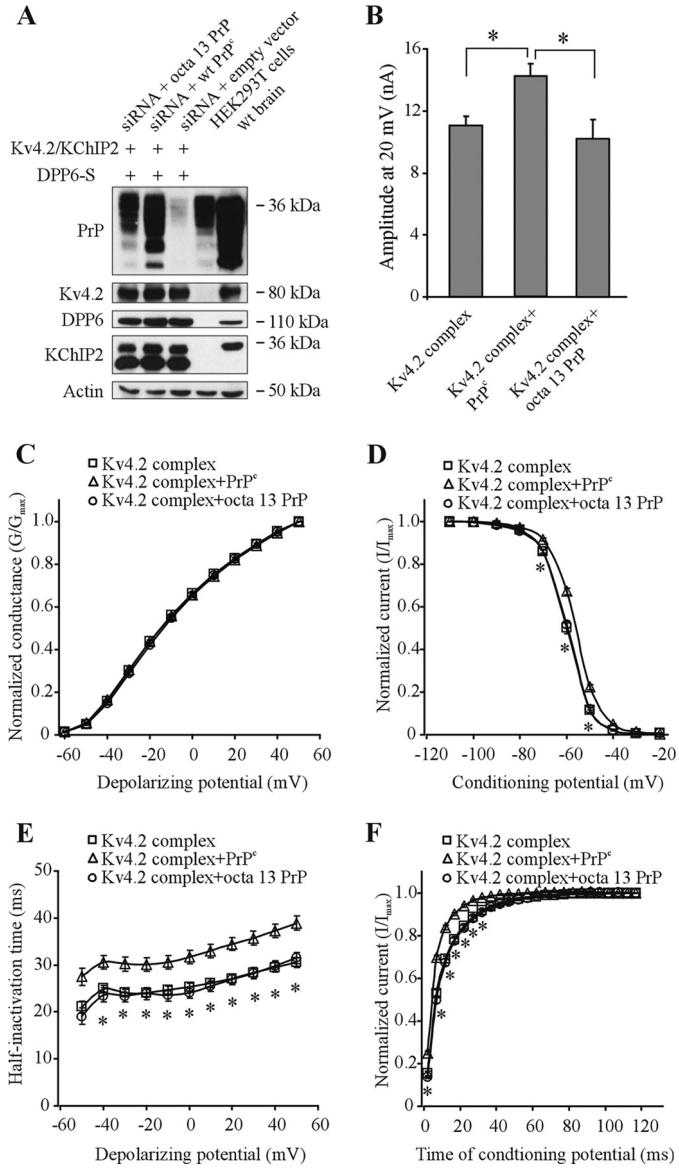

FIGURE 9. **Expansion of PrP octarepeats is loss of function for effects upon Kv4.2-mediated A-type currents.** *A*, Western blots demonstrating the presence or absence of channel components. *B*, average peak amplitude of A-type K$^+$ currents at a depolarizing potential of 20 mV mediated by different Kv4.2 channel complexes, as indicated. *C–F*, averaged activation curves, steady-state inactivation curves, half-inactivation time, and recovery curves from steady-state inactivation of A-type currents mediated by Kv4.2 channel complexes. For data in *C–F*, for Kv4.2 complexes, $n = 13$; for Kv4.2 channel complex plus PrP^C, $n = 9$; and for Kv4.2 channel complex plus octa13 PrP, $n = 12$. Channel compositions in traces are denoted within *insets*. There is no significant difference between the properties of A-type K$^+$ currents of the Kv4.2 channel complex alone and in the presence of octa13 PrP. Endogenous PrP^c was reduced by application of siRNA directed against human *PRNP*. *, significant difference (group of Kv4.2 channel complex plus exogenous PrP^C *versus* Kv4.2 channel complex plus octa13 PrP and/or Kv4.2 channel complex alone ($p < 0.05$)). *Error bars*, S.E.

only can assemble membrane proteins in a cellular signaling microenvironment but also can impact or adjust function. Findings presented here seem compatible with this proposal as can the loss-of-function phenotype of the octa13 allele in electrophysiological assays (Fig. 9). Aside from the inefficiency of octa13 PrP at forming DPP6-S-containing complexes (Fig. 4, *C* and *D*), our studies revealed that it is incapable of forming another type of complex. This effect is apparent in both RK13 and HEK293T cells (Fig. 4, *C* and *D*), where a complex of ~110 kDa containing WT PrP (indicated by *open arrows*) is absent for octa13 PrP. The ~110-kDa complex could represent a PrP^C·DPP6-S monomer complex or interaction with a different protein, as suggested by the failure to detect endogenous DPP6 in HEK293T cells (Figs. 6*A*, 9*A*, and 10*A*). In terms of potentially analogous effects for protein-protein interactions, it is notable that PrP with 14 octarepeats was loss of function for inhibiting β-cleavage of APP, whereas PrP^C without the octarepeat region retained activity (65). Although a direct physical interaction between PrP^C and the β-cleaving enzyme has been questioned (66), the concept of

TABLE 1

The properties of Kv4.2-mediated A-type currents in HEK293T cells

Activation: V_{on}, depolarizing membrane potential at which significant currents first become apparent; $V_{0.5}$, depolarizing membrane potential, in which 50% conductance of A-type currents is activated, obtained by fitting the activation curve to a first order Boltzmann function; k, slope at midpoint of the curve. Inactivation: $V_{0.5}$, conditioning membrane potential, in which 50% of the Kv4.2 channels were inactivated, obtained by fitting the inactivation curve to a first order Boltzmann function; K, slope at midpoint of the curve. Kinetics: $t_{½}$, the time at which 50% of peak amplitude is inactivated at the indicated membrane potential; τ_{rec}, time constant of recovery curve, obtained by fitting the curve to a single exponential function.

	Activation			Inactivation		Kinetics	
	V_{on}	$V_{0.5}$	k	$V_{0.5}$	k	$t_{½}$ at 40 mV	τ_{rec}
	mV			*mV*		*ms*	
siRNA + Kv4.2 +KChIP2 + DPP6-S	−58.7	−21.5 ± 2.6	26.2 ± 2.7	−60.1 ± 0.2	5.2 ± 0.2	29.5 ± 7.3	11.7 ± 0.5
siRNA + Kv4.2 +KChIP2 + DPP6-S + PrP^C	−58.8	−22.6 ± 3.1	28.3 ± 3.1	−56.3 ± 0.2	5.1 ± 0.2	37.2 ± 8.8	7.3 ± 0.3
siRNA + Kv4.2 +KChIP2 + DPP6-S + octa13 PrP	−59.1	−20.7 ± 2.1	25.2 ± 2.2	−59.8 ± 0.2	5.2 ± 0.2	29.7 ± 7.2	12.2 ± 0.5

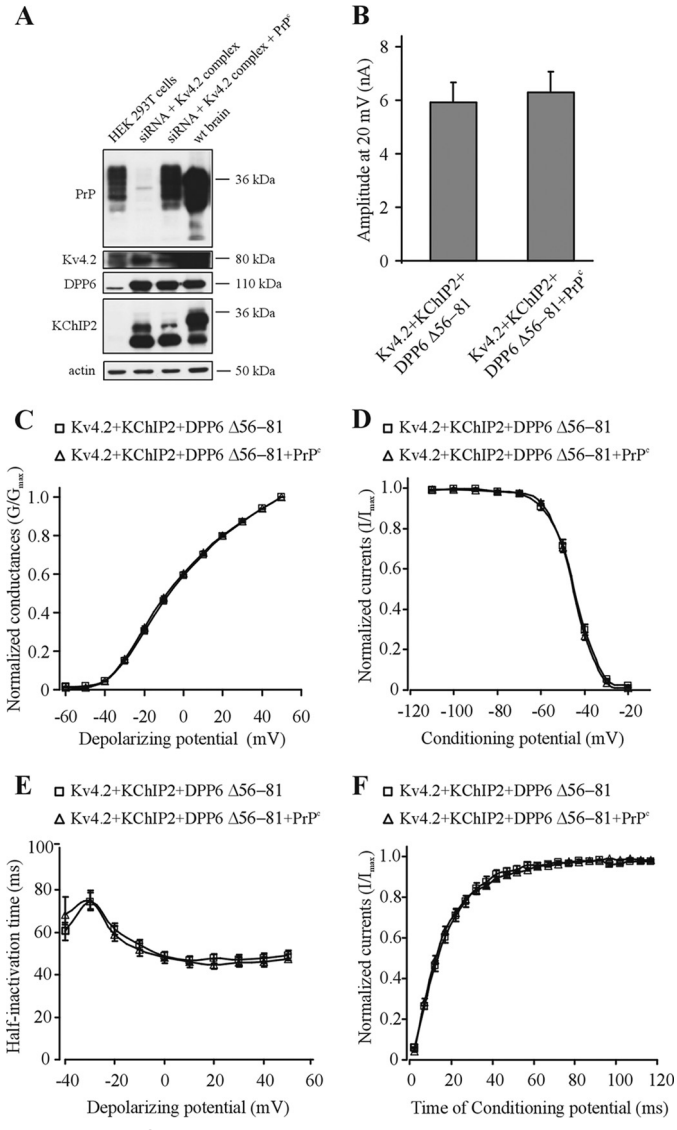

FIGURE 10. **PrP^C fails to modulate Kv4.2-mediated A-type K$^+$ currents reconstituted with DPP6 Δ56–81.** *A*, Western blots demonstrating the presence or absence of channel components. *B*, average peak amplitude of A-type K$^+$ currents at a depolarizing potential of 20 mV. *C*, average curves of voltage-dependent activation of A-type currents. *D*, averaged curves of voltage-dependent steady-state inactivation of A-type currents. *E*, averaged half-inactivation times of A-type currents. *F*, averaged curves of recovery rate from steady-state inactivation of A-type currents. For *B–F*, data are from HEK293T cells expressing Kv4.2, KChIP2, and DPP6 Δ56–81 (squares, $n = 8$) *versus* cells expressing Kv4.2, KChIP2, and DPP6 Δ56–81 with exogenous PrP^C (*triangles*; $n = 9$). Endogenous PrP^c was reduced by application of an siRNA directed against human *PRNP*. *Error bars*, S.E.

plasma membrane-signaling microdomains orchestrated by PrP^C may have considerable merit.

PrP^C, DPP6, and Neurologic Diseases—The >75% reduction in formation of ~191- and ~110-kDa complexes by octa13 PrP is notable (Fig. 4, *C* and *D*) and serves as a useful control to measure against the performance of WT PrP^C. However, two other GSS alleles tested here did not behave in the same way, and GSS pathogenesis is normally considered as "gain of function" due to misfolding of PrP. Whether the loss-of-function effect is due to an approximately one-third reduction in protein at the cell surface (50.1 ± 7.5% *versus* 78.1 ± 3.9% for octa13 *versus* WT, as measured by a biotinylation assay; not shown) is not clear. The electrophysiological observations made here apply to non-neuronal HEK293T cells, and it remains possible that excitable cells may behave differently, but given prominent expression of DPP6 and PrP^C in the CNS, where they are located in close proximity (19), our findings do broach the question as to how modulation of A-type K$^+$ currents by WT PrP^C via DPP6-S might feature within a broader spectrum of neurological diseases. Although the verdict may still be out on the DPP6 locus as a significant risk factor for autism spectrum disorders (67, 68) and ALS (69–71), other possibilities remain. WT PrP^C modifies the A-type K$^+$ currents from reconstituted Kv4.2 channel complexes by increasing peak amplitude, shifting the voltage-dependent steady-state inactivation curve to the right (more positive membrane potential), slowing inactivation, and decreasing recovery time from steady-state inactivation. This overall impact of enhancement prompts two speculations. First, enhancement plays a critical role in the down-regulation of neuronal membrane excitability and is associated with a decreased susceptibility to seizures (27, 28, 72); interestingly, a reported phenotype of *Prnp$^{0/0}$* mice is an increased vulnerability to drug-induced seizures (73, 74). Second, our previous work has established that PrP^C is essential for the modulation of neuronal excitability by Aβ oligomers in cholinergic basal forebrain neurons (75). Thus, the present findings implicate PrP^C regulation of Kv4.2 channels as a mechanism that could contribute to the observed effects of oligomeric Aβ (and perhaps other types of protein aggregate assemblies (76)) on neuronal excitability and viability.

Acknowledgments—DPP6^{df5J}/Rw mice were a generous gift from Dr. John Schimenti, and we thank Dr. Nam-Chaing Wang (Hospital for Sick Children, Toronto, Canada) for peptide syntheses. α-Thy-1 was a gift from Dr. Roger Morris (King's College, London).

REFERENCES

1. Wopfner, F., Weidenhöfer, G., Schneider, R., von Brunn, A., Gilch, S., Schwarz, T. F., Werner, T., and Schätzl, H. M. (1999) Analysis of 27 mammalian and 9 avian PrPs reveals high conservation of flexible regions of the prion protein. *J. Mol. Biol.* **289,** 1163–1178
2. Calzolai, L., Lysek, D. A., Pérez, D. R., Güntert, P., and Wüthrich, K. (2005) Prion protein NMR structures of chickens, turtles, and frogs. *Proc. Natl. Acad. Sci. U.S.A.* **102,** 651–655
3. Büeler, H., Fischer, M., Lang, Y., Bluethmann, H., Lipp, H. P., DeArmond, S. J., Prusiner, S. B., Aguet, M., and Weissmann, C. (1992) Normal development and behaviour of mice lacking the neuronal cell-surface PrP protein. *Nature* **356,** 577–582
4. Manson, J. C., Clarke, A. R., Hooper, M. L., Aitchison, L., McConnell, I., and Hope, J. (1994) 129/Ola mice carrying a null mutation in PrP that abolishes mRNA production are developmentally normal. *Mol. Neurobiol.* **8,** 121–127
5. Collinge, J., Whittington, M. A., Sidle, K. C., Smith, C. J., Palmer, M. S., Clarke, A. R., and Jefferys, J. G. (1994) Prion protein is necessary for normal synaptic function. *Nature* **370,** 295–297
6. Whittington, M. A., Sidle, K. C., Gowland, I., Meads, J., Hill, A. F., Palmer, M. S., Jefferys, J. G., and Collinge, J. (1995) Rescue of neurophysiological phenotype seen in PrP null mice by transgene encoding human prion protein. *Nat. Genet.* **9,** 197–201
7. Manson, J. C., Hope, J., Clarke, A. R., Johnston, A., Black, C., and MacLeod, N. (1995) PrP gene dosage and long term potentiation. *Neurodegeneration.* **4,** 113–114
8. Curtis, J., Errington, M., Bliss, T., Voss, K., and MacLeod, N. (2003) Age-dependent loss of PTP and LTP in the hippocampus of PrP-null mice. *Neurobiol. Dis.* **13,** 55–62
9. Rieger, R., Edenhofer, F., Lasmézas, C. I., and Weiss, S. (1997) The human 37-kDa laminin receptor precursor interacts with the prion protein in eukaryotic cells. *Nat. Med.* **3,** 1383–1388
10. Gauczynski, S., Peyrin, J. M., Haïk, S., Leucht, C., Hundt, C., Rieger, R., Krasemann, S., Deslys, J. P., Dormont, D., Lasmézas, C. I., and Weiss, S. (2001) The 37-kDa/67-kDa laminin receptor acts as the cell-surface receptor for the cellular prion protein. *EMBO J.* **20,** 5863–5875
11. Hundt, C., Peyrin, J. M., Haïk, S., Gauczynski, S., Leucht, C., Rieger, R., Riley, M. L., Deslys, J. P., Dormont, D., Lasmézas, C. I., and Weiss, S. (2001) Identification of interaction domains of the prion protein with its 37-kDa/67-kDa laminin receptor. *EMBO J.* **20,** 5876–5886
12. Schmitt-Ulms, G., Legname, G., Baldwin, M. A., Ball, H. L., Bradon, N., Bosque, P. J., Crossin, K. L., Edelman, G. M., DeArmond, S. J., Cohen, F. E., and Prusiner, S. B. (2001) Binding of neural cell adhesion molecules (N-CAMs) to the cellular prion protein. *J. Mol. Biol.* **314,** 1209–1225
13. Santuccione, A., Sytnyk, V., Leshchyns'ka, I., and Schachner, M. (2005) Prion protein recruits its neuronal receptor NCAM to lipid rafts to activate p59fyn and to enhance neurite outgrowth. *J. Cell Biol.* **169,** 341–354
14. Zanata, S. M., Lopes, M. H., Mercadante, A. F., Hajj, G. N., Chiarini, L. B., Nomizo, R., Freitas, A. R., Cabral, A. L., Lee, K. S., Juliano, M. A., de Oliveira, E., Jachieri, S. G., Burlingame, A., Huang, L., Linden, R., Brentani, R. R., and Martins, V. R. (2002) Stress-inducible protein 1 is a cell surface ligand for cellular prion that triggers neuroprotection. *EMBO J.* **21,** 3307–3316
15. Roffé, M., Beraldo, F. H., Bester, R., Nunziante, M., Bach, C., Mancini, G., Gilch, S., Vorberg, I., Castilho, B. A., Martins, V. R., and Hajj, G. N. (2010) Prion protein interaction with stress-inducible protein 1 enhances neuronal protein synthesis via mTOR. *Proc. Natl. Acad. Sci. U.S.A.* **107,** 13147–13152
16. Khosravani, H., Zhang, Y., Tsutsui, S., Hameed, S., Altier, C., Hamid, J., Chen, L., Villemaire, M., Ali, Z., Jirik, F. R., and Zamponi, G. W. (2008) Prion protein attenuates excitotoxicity by inhibiting NMDA receptors. *J. Gen. Physiol.* **131,** i5
17. You, H., Tsutsui, S., Hameed, S., Kannanayakal, T. J., Chen, L., Xia, P., Engbers, J. D., Lipton, S. A., Stys, P. K., and Zamponi, G. W. (2012) Abeta neurotoxicity depends on interactions between copper ions, prion protein, and *N*-methyl-D-aspartate receptors. *Proc. Natl. Acad. Sci. U.S.A.* **109,** 1737–1742
18. Watts, J. C., and Westaway, D. (2007) The prion protein family. Diversity, rivalry, and dysfunction. *Biochim. Biophys. Acta* **1772,** 654–672
19. Schmitt-Ulms, G., Hansen, K., Liu, J., Cowdrey, C., Yang, J., DeArmond, S. J., Cohen, F. E., Prusiner, S. B., and Baldwin, M. A. (2004) Time-controlled transcardiac perfusion cross-linking for the study of protein interactions in complex tissues. *Nat. Biotechnol.* **22,** 724–731
20. Nadal, M. S., Ozaita, A., Amarillo, Y., Vega-Saenz de Miera, E., Ma, Y., Mo, W., Goldberg, E. M., Misumi, Y., Ikehara, Y., Neubert, T. A., and Rudy, B. (2003) The CD26-related dipeptidyl aminopeptidase-like protein DPPX is a critical component of neuronal A-type K^+ channels. *Neuron* **37,** 449–461
21. Kim, J., Nadal, M. S., Clemens, A. M., Baron, M., Jung, S. C., Misumi, Y., Rudy, B., and Hoffman, D. A. (2008) Kv4 accessory protein DPPX (DPP6) is a critical regulator of membrane excitability in hippocampal CA1 pyramidal neurons. *J. Neurophysiol.* **100,** 1835–1847
22. An, W. F., Bowlby, M. R., Betty, M., Cao, J., Ling, H. P., Mendoza, G., Hinson, J. W., Mattsson, K. I., Strassle, B. W., Trimmer, J. S., and Rhodes, K. J. (2000) Modulation of A-type potassium channels by a family of calcium sensors. *Nature* **403,** 553–556
23. Seikel, E., and Trimmer, J. S. (2009) Convergent modulation of Kv4.2 channel α subunits by structurally distinct DPPX and KChIP auxiliary subunits. *Biochemistry* **48,** 5721–5730
24. Maffie, J., Blenkinsop, T., and Rudy, B. (2009) A novel DPP6 isoform (DPP6-E) can account for differences between neuronal and reconstituted A-type K^+ channels. *Neurosci. Lett.* **449,** 189–194
25. Pruunsild, P., and Timmusk, T. (2005) Structure, alternative splicing, and expression of the human and mouse KCNIP gene family. *Genomics* **86,** 581–593
26. Marionneau, C., LeDuc, R. D., Rohrs, H. W., Link, A. J., Townsend, R. R., and Nerbonne, J. M. (2009) Proteomic analyses of native brain $K_V4.2$ channel complexes. *Channels* **3,** 284–294
27. Birnbaum, S. G., Varga, A. W., Yuan, L. L., Anderson, A. E., Sweatt, J. D., and Schrader, L. A. (2004) Structure and function of Kv4-family transient potassium channels. *Physiol. Rev.* **84,** 803–833
28. Johnston, D., Christie, B. R., Frick, A., Gray, R., Hoffman, D. A., Schexnayder, L. K., Watanabe, S., and Yuan, L. L. (2003) Active dendrites, potassium channels and synaptic plasticity. *Philos. Trans. R. Soc. Lond. B Biol. Sci.* **358,** 667–674
29. Sun, W., Maffie, J. K., Lin, L., Petralia, R. S., Rudy, B., and Hoffman, D. A. (2011) DPP6 establishes the A-type K^+ current gradient critical for the regulation of dendritic excitability in CA1 hippocampal neurons. *Neuron* **71,** 1102–1115
30. Lundby, A., Jespersen, T., Schmitt, N., Grunnet, M., Olesen, S. P., Cordeiro, J. M., and Calloe, K. (2010) Effect of the I(to) activator NS5806 on cloned K_V4 channels depends on the accessory protein KChIP2. *Br. J. Pharmacol.* **160,** 2028–2044
31. Witzel, K., Fischer, P., and Bähring, R. (2012) Hippocampal A-type current and Kv4.2 channel modulation by the sulfonylurea compound NS5806. *Neuropharmacology* **63,** 1389–1403
32. Chomczynski, P., and Sacchi, N. (1987) Single-step method of RNA isolation by acid guanidinium thiocyanate-phenol-chloroform extraction. *Anal. Biochem.* **162,** 156–159
33. Drisaldi, B., Coomaraswamy, J., Mastrangelo, P., Strome, B., Yang, J., Watts, J. C., Chishti, M. A., Marvi, M., Windl, O., Ahrens, R., Major, F., Sy, M. S., Kretzschmar, H., Fraser, P. E., Mount, H. T., and Westaway, D. (2004) Genetic mapping of activity determinants within cellular prion proteins. N-terminal modules in PrPC offset pro-apoptotic activity of the Doppel helix B/B′ region. *J. Biol. Chem.* **279,** 55443–55454
34. Hough, R. B., Lengeling, A., Bedian, V., Lo, C., and Bućan, M. (1998) Rump white inversion in the mouse disrupts dipeptidyl aminopeptidase-like protein 6 and causes dysregulation of Kit expression. *Proc. Natl. Acad. Sci. U.S.A.* **95,** 13800–13805
35. Strop, P., Bankovich, A. J., Hansen, K. C., Garcia, K. C., and Brunger, A. T. (2004) Structure of a human A-type potassium channel interacting protein DPPX, a member of the dipeptidyl aminopeptidase family. *J. Mol. Biol.* **343,** 1055–1065
36. Clark, B. D., Kwon, E., Maffie, J., Jeong, H. Y., Nadal, M., Strop, P., and Rudy, B. (2008) DPP6 localization in brain supports function as a Kv4

channel associated protein. *Front. Mol. Neurosci.* **1,** 8
37. Homans, S. W., Ferguson, M. A., Dwek, R. A., Rademacher, T. W., Anand, R., and Williams, A. F. (1988) Complete structure of the glycosyl phosphatidylinositol membrane anchor of rat brain Thy-1 glycoprotein. *Nature* **333,** 269–272
38. Riek, R., Hornemann, S., Wider, G., Billeter, M., Glockshuber, R., and Wüthrich, K. (1996) NMR structure of the mouse prion protein domain PrP(121–231). *Nature* **382,** 180–182
39. Riek, R., Hornemann, S., Wider, G., Glockshuber, R., and Wüthrich, K. (1997) NMR characterization of the full-length recombinant murine prion protein, mPrP(23–231). *FEBS Lett.* **413,** 282–288
40. Mo, H., Moore, R. C., Cohen, F. E., Westaway, D., Prusiner, S. B., Wright, P. E., and Dyson, H. J. (2001) Two different neurodegenerative diseases caused by proteins with similar structures. *Proc. Natl. Acad. Sci. U.S.A.* **98,** 2352–2357
41. Laplanche, J. L., Hachimi, K. H., Durieux, I., Thuillet, P., Defebvre, L., Delasnerie-Laupretre, N., Peoc'h, K., Foncin, J. F., and Destee, A. (1999) Prominent psychiatric features and early onset in an inherited prion disease with a new insertional mutation in the prion protein gene. *Brain* **122,** 2375–2386
42. Doh-ura, K., Tateishi, J., Sasaki, H., Kitamoto, T., and Sakaki, Y. (1989) Pro–Leu change at position 102 of prion protein is the most common but not the sole mutation related to Gerstmann-Straussler syndrome. *Biochem. Biophys. Res. Commun.* **163,** 974–979
43. Hsiao, K. K., Cass, C., Schellenberg, G. D., Bird, T., Devine-Gage, E., Wisniewski, H., and Prusiner, S. B. (1991) A prion protein variant in a family with the telencephalic form of Gerstmann-Straussler-Scheinker syndrome. *Neurology* **41,** 681–684
44. Hinnell, C., Coulthart, M. B., Jansen, G. H., Cashman, N. R., Lauzon, J., Clark, A., Costello, F., White, C., Midha, R., Wiebe, S., and Furtado, S. (2011) Gerstmann-Straussler-Scheinker disease due to a novel prion protein gene mutation. *Neurology* **76,** 485–487
45. Oesch, B., Westaway, D., Wälchli, M., McKinley, M. P., Kent, S. B., Aebersold, R., Barry, R. A., Tempst, P., Teplow, D. B., and Hood, L. E. (1985) A cellular gene encodes scrapie PrP 27–30 protein. *Cell* **40,** 735–746
46. Kretzschmar, H. A., Prusiner, S. B., Stowring, L. E., and DeArmond, S. J. (1986) Scrapie prion proteins are synthesized in neurons. *Am. J. Pathol.* **122,** 1–5
47. Peralta, O. A., and Eyestone, W. H. (2009) Quantitative and qualitative analysis of cellular prion protein (PrP(C)) expression in bovine somatic tissues. *Prion* **3,** 161–170
48. Herms, J. W., Tings, T., Dunker, S., and Kretzschmar, H. A. (2001) Prion protein affects Ca^{2+}-activated K^+ currents in cerebellar purkinje cells. *Neurobiol. Dis.* **8,** 324–330
49. Carleton, A., Tremblay, P., Vincent, J. D., and Lledo, P. M. (2001) Dose-dependent, prion protein (PrP)-mediated facilitation of excitatory synaptic transmission in the mouse hippocampus. *Pflugers Arch.* **442,** 223–229
50. Mallucci, G. R., Ratté, S., Asante, E. A., Linehan, J., Gowland, I., Jefferys, J. G., and Collinge, J. (2002) Post-natal knockout of prion protein alters hippocampal CA1 properties, but does not result in neurodegeneration. *EMBO J.* **21,** 202–210
51. Prestori, F., Rossi, P., Bearzatto, B., Lainé, J., Necchi, D., Diwakar, S., Schiffmann, S. N., Axelrad, H., and D'Angelo, E. (2008) Altered neuron excitability and synaptic plasticity in the cerebellar granular layer of juvenile prion protein knock-out mice with impaired motor control. *J. Neurosci.* **28,** 7091–7103
52. Yu, S. P., and Kerchner, G. A. (1998) Endogenous voltage-gated potassium channels in human embryonic kidney (HEK293) cells. *J. Neurosci. Res.* **52,** 612–617
53. Jiang, B., Sun, X., Cao, K., and Wang, R. (2002) Endogenous Kv channels in human embryonic kidney (HEK-293) cells. *Mol. Cell. Biochem.* **238,** 69–79
54. Solomon, I. H., Huettner, J. E., and Harris, D. A. (2010) Neurotoxic mutants of the prion protein induce spontaneous ionic currents in cultured cells. *J. Biol. Chem.* **285,** 26719–26726
55. Solomon, I. H., Khatri, N., Biasini, E., Massignan, T., Huettner, J. E., and Harris, D. A. (2011) An N-terminal polybasic domain and cell surface localization are required for mutant prion protein toxicity. *J. Biol. Chem.* **286,** 14724–14736
56. Colling, S. B., Collinge, J., and Jefferys, J. G. (1996) Hippocampal slices from prion protein null mice. Disrupted Ca^{2+}-activated K^+ currents. *Neurosci. Lett.* **209,** 49–52
57. Powell, A. D., Toescu, E. C., Collinge, J., and Jefferys, J. G. (2008) Alterations in Ca^{2+}-buffering in prion-null mice. Association with reduced afterhyperpolarizations in CA1 hippocampal neurons. *J. Neurosci.* **28,** 3877–3886
58. Beraldo, F. H., Arantes, C. P., Santos, T. G., Queiroz, N. G., Young, K., Rylett, R. J., Markus, R. P., Prado, M. A., and Martins, V. R. (2010) Role of α7 nicotinic acetylcholine receptor in calcium signaling induced by prion protein interaction with stress-inducible protein 1. *J. Biol. Chem.* **285,** 36542–36550
59. Watt, N. T., Taylor, D. R., Kerrigan, T. L., Griffiths, H. H., Rushworth, J. V., Whitehouse, I. J., and Hooper, N. M. (2012) Prion protein facilitates uptake of zinc into neuronal cells. *Nat. Commun.* **3,** 1134
60. Hornemann, S., Korth, C., Oesch, B., Riek, R., Wider, G., Wüthrich, K., and Glockshuber, R. (1997) Recombinant full-length murine prion protein, mPrP(23–231). Purification and spectroscopic characterization. *FEBS Lett.* **413,** 277–281
61. Muramoto, T., DeArmond, S. J., Scott, M., Telling, G. C., Cohen, F. E., and Prusiner, S. B. (1997) Heritable disorder resembling neuronal storage disease in mice expressing prion protein with deletion of an α-helix. *Nat. Med.* **3,** 750–755
62. Watts, J. C., Huo, H., Bai, Y., Ehsani, S., Jeon, A. H., Won, A. H., Shi, T., Daude, N., Lau, A., Young, R., Xu, L., Carlson, G. A., Williams, D., Westaway, D., and Schmitt-Ulms, G. (2009) Interactome analyses identify ties of PrP and its mammalian paralogs to oligomannosidic *N*-glycans and endoplasmic reticulum-derived chaperones. *PLoS Pathog.* **5,** e1000608
63. Ren, X., Hayashi, Y., Yoshimura, N., and Takimoto, K. (2005) Transmembrane interaction mediates complex formation between peptidase homologues and Kv4 channels. *Mol. Cell. Neurosci.* **29,** 320–332
64. Linden, R., Martins, V. R., Prado, M. A., Cammarota, M., Izquierdo, I., and Brentani, R. R. (2008) Physiology of the prion protein. *Physiol. Rev.* **88,** 673–728
65. Parkin, E. T., Watt, N. T., Hussain, I., Eckman, E. A., Eckman, C. B., Manson, J. C., Baybutt, H. N., Turner, A. J., and Hooper, N. M. (2007) Cellular prion protein regulates β-secretase cleavage of the Alzheimer's amyloid precursor protein. *Proc. Natl. Acad. Sci. U.S.A.* **104,** 11062–11067
66. McHugh, P. C., Wright, J. A., Williams, R. J., and Brown, D. R. (2012) Prion protein expression alters APP cleavage without interaction with BACE-1. *Neurochem. Int.* **61,** 672–680
67. Noor, A., Whibley, A., Marshall, C. R., Gianakopoulos, P. J., Piton, A., Carson, A. R., Orlic-Milacic, M., Lionel, A. C., Sato, D., Pinto, D., Drmic, I., Noakes, C., Senman, L., Zhang, X., Mo, R., Gauthier, J., Crosbie, J., Pagnamenta, A. T., Munson, J., Estes, A. M., Fiebig, A., Franke, A., Schreiber, S., Stewart, A. F., Roberts, R., McPherson, R., Guter, S. J., Cook, E. H., Jr., Dawson, G., Schellenberg, G. D., Battaglia, A., Maestrini, E., Autism Genome Project Consortium, Jeng, L., Hutchison, T., Rajcan-Separovic, E., Chudley, A. E., Lewis, S. M., Liu, X., Holden, J. J., Fernandez, B., Zwaigenbaum, L., Bryson, S. E., Roberts, W., Szatmari, P., Gallagher, L., Stratton, M. R., Gecz, J., Brady, A. F., Schwartz, C. E., Schachar, R. J., Monaco, A. P., Rouleau, G. A., Hui, C. C., Lucy Raymond, F., Scherer, S. W., and Vincent, J. B. (2010) Disruption at the PTCHD1 locus on Xp22.11 in autism spectrum disorder and intellectual disability. *Sci. Transl. Med.* **2,** 49ra68
68. Marshall, C. R., Noor, A., Vincent, J. B., Lionel, A. C., Feuk, L., Skaug, J., Shago, M., Moessner, R., Pinto, D., Ren, Y., Thiruvahindrapduram, B., Fiebig, A., Schreiber, S., Friedman, J., Ketelaars, C. E., Vos, Y. J., Ficicioglu, C., Kirkpatrick, S., Nicolson, R., Sloman, L., Summers, A., Gibbons, C. A., Teebi, A., Chitayat, D., Weksberg, R., Thompson, A., Vardy, C., Crosbie, V., Luscombe, S., Baatjes, R., Zwaigenbaum, L., Roberts, W., Fernandez, B., Szatmari, P., and Scherer, S. W. (2008) Structural variation of chromosomes in autism spectrum disorder. *Am. J. Hum. Genet.* **82,** 477–488
69. van Es, M. A., van Vught, P. W., Blauw, H. M., Franke, L., Saris, C. G., Van den Bosch, L., de Jong, S. W., de Jong, V., Baas, F., van't Slot, R., Lemmens, R., Schelhaas, H. J., Birve, A., Sleegers, K., Van Broeckhoven, C., Schymick, J. C., Traynor, B. J., Wokke, J. H., Wijmenga, C., Robberecht, W., Andersen, P. M., Veldink, J. H., Ophoff, R. A., and van den Berg, L. H. (2008)

Genetic variation in DPP6 is associated with susceptibility to amyotrophic lateral sclerosis. *Nat. Genet.* **40,** 29–31

70. Cronin, S., Berger, S., Ding, J., Schymick, J. C., Washecka, N., Hernandez, D. G., Greenway, M. J., Bradley, D. G., Traynor, B. J., and Hardiman, O. (2008) A genome-wide association study of sporadic ALS in a homogenous Irish population. *Hum. Mol. Genet.* **17,** 768–774
71. Fogh, I., D'Alfonso, S., Gellera, C., Ratti, A., Cereda, C., Penco, S., Corrado, L., Sorarù, G., Castellotti, B., Tiloca, C., Gagliardi, S., Cozzi, L., Lupton, M. K., Ticozzi, N., Mazzini, L., Shaw, C. E., Al-Chalabi, A., Powell, J., and Silani, V. (2011) No association of DPP6 with amyotrophic lateral sclerosis in an Italian population. *Neurobiol. Aging* **32,** 966–967
72. Fransén, E., and Tigerholm, J. (2010) Role of A-type potassium currents in excitability, network synchronicity, and epilepsy. *Hippocampus* **20,** 877–887
73. Walz, R., Amaral, O. B., Rockenbach, I. C., Roesler, R., Izquierdo, I., Cavalheiro, E. A., Martins, V. R., and Brentani, R. R. (1999) Increased sensitivity to seizures in mice lacking cellular prion protein. *Epilepsia* **40,** 1679–1682
74. Rangel, A., Burgaya, F., Gavín, R., Soriano, E., Aguzzi, A., and Del Río, J. A. (2007) Enhanced susceptibility of Prnp-deficient mice to kainate-induced seizures, neuronal apoptosis, and death. Role of AMPA/kainate receptors. *J. Neurosci. Res.* **85,** 2741–2755
75. Alier, K., Ma, L., Yang, J., Westaway, D., and Jhamandas, J. H. (2011) Aβ inhibition of ionic conductance in mouse basal forebrain neurons is dependent upon the cellular prion protein PrPC. *J. Neurosci.* **31,** 16292–16297
76. Resenberger, U. K., Harmeier, A., Woerner, A. C., Goodman, J. L., Müller, V., Krishnan, R., Vabulas, R. M., Kretzschmar, H. A., Lindquist, S., Hartl, F. U., Multhaup, G., Winklhofer, K. F., and Tatzelt, J. (2011) The cellular prion protein mediates neurotoxic signalling of β-sheet-rich conformers independent of prion replication. *EMBO J.* **30,** 2057–2070